Submitted to Progress in Oceanography on September 29, 2011

The Mediterranean Sea in- and out-flows' heterogeneities

Claude Millot
Laboratoire d'Océanographie Physique Biogéochimique
Antenne LOPB-COM-CNRS de La Seyne/mer, BP 330, F-83150
f4eut@winlink.org and ailesetiles@gmail.com

Abstract

This paper is a development of a companion one, published two years ago in the same journal, which proposed another concept of the Mediterranean Sea outflow through the Strait of Gibraltar. While other papers about the outflow assume that it is composed of only two Mediterranean Waters (MWs), the Levantine Intermediate Water (LIW) and the Western Mediterranean Deep Water (WMDW) from the eastern and western basins, respectively, we found evidence, from a re-analysis of 1985-1986 CTD profiles (Gibraltar Experiment, GIBEX), for two other MWs, the Winter Intermediate Water (WIW) from the western basin and the Tyrrhenian Dense Water (TDW) basically originated from the eastern basin. We also analyzed 2003-2008 time series from two CTDs moored (CIESM HYDROCHANGES Programme) at the southern sill of Camarinal (270 m) and on the shelf of Morocco (80 m) and we argued for a series of new ideas. Essentially, we hypothesized that, at the entrance of the strait, these four MWs are roughly laying one above the other in proportions varying from north to south. Then, while progressing westward, the isopycnals associated with these MWs tilt up southward as much as being, within the strait, roughly parallel to the continental slope of Morocco where the densest MWs are. The MWs in the strait are thus juxtaposed and they all mix with one or the other of the two Atlantic Water components (so that the inflow acronym is AWs), the Surface Atlantic Water (SAW) and the North Atlantic Central Water (NACW). This leads to an outflow that is horizontally heterogeneous before progressively becoming vertically heterogeneous, then leading to a splitting into a series of superimposed veins.

Meanwhile, comparing the previous CTD time series with another one collected simultaneously at the southern sill of Espartel (by the University of Malaga, still within the CIESM HYDROCHANGES Programme and with Spanish funds from INGRES projects) has recently allowed us demonstrating the significance of mixing lines computed from two successive records. Luckily, the CTDs moored at the two sills are generally located roughly along the same streamline so that the along-stream evolution of the MWs outflowing there can be monitored. The outflow, which does not show any clear seasonal variability before entering the strait, strongly mixes within the strait, due mainly to the internal tide, with the seasonally variable inflow so that it gets marked seasonal and fortnightly variabilities within the strait. A major general result is that, since both the outflow and the inflow display marked spatial heterogeneity and both long-term and short-term temporal variabilities before they mix, accurately predicting the characteristics of the outflow into the ocean appears almost impossible. Another major result is that we demonstrated the possibility to link, under some

conditions, two sets of data collected at different locations along the strait, such as for instance CTD profiles collected at different longitudes.

Because there is still some reticence in accepting our concept of the Mediterranean Sea outflow and some of our hypotheses could be considered as too subjective, we propose herein a fully objective description of the water masses distribution during the GIB1 and GIB2 campaigns of GIBEX. Where the AWs and the MWs do not markedly mix, each of them is defined in terms of density and temperature ranges. Where a MW mixes with one of the AWs down to the bottom, the mixing line characteristics allow following that MW from one section to the other downstream; note that the notion "down to the bottom" is essential since, otherwise, the mixing line characteristics will change as the mixing deepens. We clearly demonstrate that the various MWs, or at least the various waters defined, at anybody's convenience, with a series of density and temperature ranges, follow the general concept we have proposed. Being superimposed before entering the strait, they come to be juxtaposed within the strait before becoming superimposed again.

Additionally, we have had the opportunity to analyse additional CTD time series collected by the University of Malaga on both south and north sides of the southern sill of Espartel. We clearly demonstrate herein that, even though the MWs outflowing at the sill and on the lower part of the southern / Moroccan slope are roughly the same, the densest ones outflow along the slope, i.e. at depths shallower than at the sill. We also clearly demonstrate that, at least during the experiment, the MWs outflowing on the lower part of the northern slope were very different from the MWs outflowing at the sill and that each mixed with different AWs. Moreover, we clearly demonstrate that, using the mixing lines computed from each time series, the data recorded at the southern sill of Espartel and on the lower part of the southern slope there allow retrieving, with a very satisfying accuracy, the data recorded at the southern sill of Camarinal, which is clearly not the case for the data recorded on the lower part of the northern slope at the southern sill of Espartel.

Having described the AWs and MWs heterogeneities within the Strait of Gibraltar, we emphasize how different they are, basically due to the different processes leading to either the inflow or the outflow. The inflow is sucked into the sea, due to the water budget (E-P) deficit in the sea, so that any type of AW present on the western entrance of the strait can enter the sea, at any time and any specific location. On the contrary, the outflow is a product of the sea that is a machine producing, in very specific places, mainly through open-sea dense water formation processes, a series of MWs that then circulate within the sea as alongslope density currents before entering the eastern side of the strait in a specific order, being driven by specific forces. We have tried schematizing what were the consequences for the mixing processes between the AWs and the MWs. We have also tried schematizing our one understanding of the Mediterranean Sea outflow.

Thanks to the demonstration we recently made of the significance of mixing lines inferred from CTD time series, the fully objective re-analysis of the GIBEX CTD profiles that anyone can make with his/her own density and temperature ranges, and the multiplication of CTD time series collected within HYDROCHANGES, definitively support the validity of the concept we proposed two years ago. In particular, it is now clearly demonstrated that the Mediterranean Sea outflow remains heterogeneous while crossing the Strait of Gibraltar, and that each of the MWs can mix with one or the other components of the Mediterranean Sea inflow. While the lightest MWs remain along the continental slope of Spain, the densest ones outflow along the continental slope of Morocco. To be noticed is that, not considering the difficulty of the working conditions within such a strait that is only ~10 km wide at about mid-depth in its narrowest part, having up to four MWs outflowing side by side there and mixing with two AWs that have a very heterogeneous and variable distribution clearly leads to a spatial heterogeneity that is actually much larger than the one evidenced herein from a relatively low number of CTD profiles and time series.

Keywords: Mediterranean Sea, Strait of Gibraltar, Circulation, Water masses

-----

List of Contents

-----

1. Introduction

This paper can be considered as the development of a companion paper (Millot, 2009; M09 hereafter) which proposed, in the same journal, another concept of the Mediterranean Sea outflow. Since historical papers about the Strait of Gibraltar, as well as a confrontation between current and personal thoughts were already presented in detail, the reader is kindly asked to read the Introduction of M09 first in order to have a full overview of the problem. Also, we apologize for citing mainly our own references, which is simply due to the fact that none of the other references supports our personal thoughts and we do not want to openly criticize them. Briefly, the outflow through the Strait of Gibraltar has been historically considered as composed of only two out of four major Mediterranean Waters (MWs) that are expected to be mixed near 6°W, thereby producing a rather homogeneous outflow that then splits into veins, due to its cascading along different paths and to different mixing conditions with the Atlantic Water (AW). Note that these considerations about a homogeneous outflow can result from incapacity to understand the heterogeneity evidenced by the data sets, and that no analysis is available about what could be the different paths and how could they induce heterogeneity then. Whatever the case, these considerations are supported neither by the analyses we have been conducting for a while about the functioning of the Mediterranean Sea nor by those we have undertaken about the strait itself.

Our own concept is that, in the westernmost part of the sea (Fig.1), intermediate MWs (the Winter Intermediate Water, WIW, the Levantine Intermediate Water, LIW, and the upper part of the Tyrrhenian Dense Water, TDWi) circulate alongslope counterclockwise due to the Coriolis effect, thus entering the strait along its northern slope one above the other. In the Alboran subbasin, the deep MWs (TDWd and WMDW, the Western Mediterranean Deep Water) circulate only sluggishly and are mainly pushed by the intermediate MWs off the southern slope where they are in direct contact with AW and thus mix noticeably with it. Since the bathymetric sections become constricted when entering the strait, intermediate MWs accelerate so that their interface with the deep MWs tilts up southward, hence easing the lifting of the latter. Schematically, the MWs that are superimposed in the sea thus come to be juxtaposed in the strait, the denser outflowing along the slope of Morocco and each of them mixing directly with AW. Since the bathymetric section widens when leaving the strait, the mixed MWs decelerate and their interface first flattens. Then, each mixed MW progressively cascades down to its specific level of equilibrium before flowing independently from the others along the Iberian slope. In the ocean, the outflow is thus structured in a number of veins, each of them being mainly dependent on the composition of the outflow in terms of MWs when entering the strait and on its interactions with the inflow within the strait. Our aim with this paper is thus to document the spatial heterogeneities of the MWs outflow, and of the AW inflow too, which justifies the use of the AWs acronym in the studied area, and demonstrate that they coherently evolve in space, both across and along the strait.

This concept was illustrated by M09 mainly from a re-analysis of CTD profiles collected during several campaigns of the 1985-1986 Gibraltar Experiment GIBEX that repeated several times a series of north-south CTD transects across the Alboran subbasin, the Strait of Gibraltar and the Gulf of Cadiz (Fig. 1). The LYNCH-702-86 (November 1985), GIB1 (March-April 1986) and GIB2 (September-October 1986) data available in the MEDATLAS database (MEDAR group, 2002) with pressure intervals of 2 dbar for GIB1,2 and 1 dbar for LYNCH are of particular interest. All these transects were performed with relatively small sampling intervals, ranging from ~2 nm (nautical miles, sometimes less) in the strait to ~3 nm outside of it, generally down to a few metres above the bottom, and as rapidly as possible.

The specific interest of the LYNCH data was already specified (Millot, 2008; summarized in M09): even though transects only focused on the strait itself, they were repeated several times within two weeks from 5°15'W to 6°05'W that were assumed to be the strait entrance and outlet for the MWs. Almost exceptionally, marked changes occurred during the campaign in the composition of both the set of MWs east of the strait and the set of AWs in the whole area, which leaded to a huge variability on a few-day time scale. We demonstrated that, strangely, the outflow overall characteristics west of the strait depend less on the set of MWs east of the strait than on the set of AWs within the strait.

The GIB1 and GIB2 transects are interesting too because they covered the whole study area within one week. The longest deepest transects (4°30'W, 5°00'W, 5°15'W) were completed in 10-15 h and the shortest shallowest ones (5°30'W, 5°40'W, 5°50'W, 6°05'W, 6°15'W) in 4-6 h. The indicated features suggest relatively stable dynamical regimes during both campaigns, making them suitable for a description of the outflow, and significant differences between them illustrate some aspects of the variability. As done by all previous authors, we considered that these transects are representative of a synoptic situation and do not depend on the relatively important tidal mixing variability with time. As usually, we thus considered only the mixing variability with space. All available transects in potential temperature (θ), salinity (S) and potential density (σ) as well as θ-S diagrams were analysed by M09, and profiles were classified according to the relative amount of light/intermediate MWs they evidence, which can be considered as too subjective. This point partly motivated the fully objective and complementary, although self sufficient, analysis of the GIB1,2 data proposed in chapter 2.

M09 also analysed CTD time series collected with autonomous CTDs (Sea-Bird SBE37-SMs) moored in key places of the whole sea in the framework of the CIESM HYDROCHANGES Programme we initiated in the early 2000s (see M09 for details about the CTD performances). Within the strait (Fig.1, 2), CTDs are serviced by the Commission pour l'Exploration Scientifique de la mer Méditerranée (CIESM), the Centre d'Océanologie de Marseille (COM) and the Service Hydrographique et Océanographique de la Marine Royale du Maroc (SHOMAR) since January 2003 at the southern sill of Camarinal (point C) and on the shelf of Morocco (point M). The University of Malaga (UMA) services another CTD at the southern sill of Espartel (point E) since September 2004 and deployed similar CTDs for limited periods at ES (Espartel-South; 128 days in October 2007-March 2008) and EN (Espartel-North; 64 days in October-December 2008); these CTDs are operated within the HYDROCHANGES programme too and are supported by the Spanish-funded INGRES projects. Results already obtained from the C, M and E time series that will not be illustrated by the data presented in chapter 3 will be summarized after the presentation of the basic ideas and hypotheses used in the whole paper.

One improvement we make as compared to M09 is to better justify how to define the AWs-MWs interface. Indeed, we did not previously realize that, for most profiles, mainly S(z) but also (and coherently) σ(z) display a maximum gradient within a range of a few tens of metres. Visually, and as objectively as possible, we specified the depth of that maximum gradient (the yellow thick line plotted in the density sections presented in chapter 2) and realized that, during both GIB1 and GIB2 and at all transects except the 6°15'W one, it nearly corresponds to the 28.0 $kg.m^{-3}$ isopycnal that is thus generally associated with the AWs-MWs interface (the 27.8 $kg.m^{-3}$ isopycnal is chosen at 6°15'W). Even though M09 choose the 28.75 $kg.m^{-3}$ isopycnal east of the sill of Camarinal and the 27.0 $kg.m^{-3}$ isopycnal west of it, all isopycnals are plotted on the sections and it can be noticed that this does not markedly change any of our results. This remark about the relative importance of the AWs-MWs interface definition applies to all other definitions of density and temperature ranges here below.

Let us first consider the θ-S diagrams in Fig.3a that focus on the AWs (σ<28.0 $kg.m^{-3}$). The two of them represented with cyan, cyan-blue and green dots are those of profiles 3 and 4 from the GIB2 transect at 6°05'W (see chapter 2). They are located only 0.9 nm (~1.7 km) apart but, although they are very similar at the surface, they are dramatically different at depth. There, profile 3 displays θ and S minima associated with NACW (the North Atlantic Central Water), even though values do not necessarily match those given in the literature (see M09), while profile 4 displays a relatively straight mixing line with the MWs. In order to present an analysis as objective as possible (necessarily specific to the GIB1 and GIB2 data sets), to identify the NACW core and give it some significant thickness, and to take into account the large seasonal variability of the Surface Atlantic Water SAW (i.e. GIB1 vs. GIB2), we arbitrarily define by σ=26.9 kg.m^{-3} the limit between NACW and SAW. Therefore, all profiles that display θ and S minima in the σ range 26.9-28.0 kg.m^{-3} will be coloured in green and all profiles in the range σ<26.9 kg.m^{-3} will be coloured in cyan. Logically, all profiles that do not display a θ minimum (a S minimum was always observed during GIB1,2) in the σ range 26.9-28.0 kg.m^{-3}, hence that do not evidence any NACW, will be coloured in cyan. The profile with grey dots comes from the same transect during the LYNCH campaign and illustrates the huge variability that can be encountered in the AWs layer, as well as the consequences for the characteristics of the outflow of mixed MWs. Figures in chapter 2 show that no GIB1,2 profile resembles the LYNCH one, i.e. without any θ or S minimum, and that SAW and NACW can no more be differentiated in the eastern Alboran, so that one deals with AW within the sea.

Let us then consider the θ-S diagram in Fig.3b that focuses on the MWs (σ>28.0 kg.m^{-3}) and is that of profile 6 from the GIB2 transect at 4°30'W. Even though such a diagram appeared relatively complex to the scientists who conducted and analysed GIBEX, since none of them correctly identified the various MWs evidenced here, as well as to the scientists that have been interested up to now in the strait dynamics, since most of them are still reticent in accepting our analysis, let us specify that such a diagram is very classic for all scientists working in the western basin of the sea. Briefly, because detailed explanations can be found in M09 together with a schematization (as Fig.2) of our own understanding of the circulation and major processes there (see Millot, 1999, for more details), let us describe the four MWs evidenced in such a diagram.

The WIW, characterised by a θ minimum, results from the AW wintertime cooling (as evidenced herein, SAW and NACW can no more be identified within the sea) in the northern part of the western basin (the Liguro-Provençal subbasin) without any mixing with the MWs below. The LIW, formed in the eastern part of the eastern basin (the Levantine subbasin), results from the AW wintertime cooling without any mixing with the MWs below. LIW has always been said to be characterised by a θ relative maximum and an S absolute maximum, but we recently suggested that this could result from a general misunderstanding of the mixing processes between LIW and the surrounding waters (Millot, submitted). Let us first note that, even thought i) it is obvious that deep MWs are also formed in the eastern basin, more especially in the Aegean and Adriatic subbasins, and ii) all studies performed as regard to the Eastern Mediterranean Transient are widely accepted, the fact that these deep eastern MWs necessarily escape the eastern basin and circulate in the western one is generally ignored. This feature was first evidenced by Millot (1999) who, considering that these deep eastern MWs cascade from the Channel of Sicily in the Tyrrhenian subbasin while mixing with the MWs resident there, named them the TDW. As illustrated by Fig.3 of Millot (submitted), the θ-S diagram in Fig.3b and the analysis herein, as well as because of the various characteristics of the four MWs, associating the S maximum with LIW would consist in giving LIW an unrealistic large amount as compared to that of TDW. Finally, the densest of the MWs in the western basin is the WMDW that is formed in the Liguro-Provençal subbasin by wintertime convection processes over the whole depth, then involving all other MWs there.

These four MWs, which necessarily mix on the vertical at least and thus form a continuum in such a θ-S diagram, can be separated only arbitrarily, what we did as objectively as possible. Whatever the case, and as said for the AWs, the density and temperature ranges we have chosen for the MWs can be modified without markedly changing the results. As long as such a θ-S diagram does not display a mixing line between one MW and one AW, we associate:

-WIW with all data that display a θ minimum in the σ range 28.0-29.0 kg.m^{-3} and colour these data in orange (note that the physics can be forgiven: data in the range … are coloured in …),

-LIW with all data that display a θ maximum in the σ range 29.0-29.075 kg.m^{-3} and colour these data in red; papers assuming that the outflow is composed of only two MWs (and the inflow of only one AW) generally link the WIW θ minimum with a AW-LIW interface. Note that the limit chosen to separate WIW from LIW (the 29.0 kg.m^{-3} isopycnal) is roughly located at mid-distance of the two θ relative extrema.

-TDW with all data in the σ range > 29.075 kg.m^{-3} and θ range >12.85 °C, and colour these data in magenta. Note that σ=29.08 kg.m^{-3}, which was chosen by M09 as the interface between the intermediate and deep MWs up to 5°40'W, hence for calculations linking the speed, the bathymetric section and the slope of the interface, is thus generally associated with TDW and is consistent with the idea that the upper/intermediate part of TDW (TDWi) circulates significantly alongslope counterclockwise while its lower/deep part (TWDd) circulates only sluggishly before being uplifted, as WMDW and as schematized in Fig.1.

-WMDW with all data in the θ range <12.85 °C (the associated σ range is generally > 29.075 kg.m^{-3}) and colour these data in blue. Papers assuming an outflow composed of only two MWs fix the LIW-WMDW interface somewhere between the two θ extrema that characterize both MWs, and below the S maximum associated with LIW in all previous papers (including ours); for instance, Kinder and Parrilla (1987) chose 12.90 °C.

When such a θ-S diagram displays a relatively straight mixing line between one MW and one AW over the whole depth, or does not evidence the MWs normally found above that MW, all data are plotted with the colour of that MW, whatever the σ and θ ranges are. This is illustrated in Fig.3b by the schematic straight mixing lines associated with WIW, LIW and WMDW; the specific illustration for TDW is described below. For instance, in case of a mixing between WMDW and SAW, which is relatively frequent in the southern part of the Alboran subbasin, data will thus be plotted in cyan for σ<28.0 kg.m^{-3} and in blue for σ>28.0 kg.m^{-3}. It is essential to understand that, where two mixing lines, or a mixing line and an unmixed (with the AWs) diagram intersect, hence defining a specific θ-S-σ set of values, only considering that specific θ-S-σ set of values does not allow characterizing which kind of MW is involved. Let us now summarize the major results already obtained from the CTD time series analysis.

The 2003-2004 time series at point C (Fig.2) and other ones from previous experiments indicate (Millot et al., 2006) that the outflowing MWs have been temporarily warming and becoming more saline since the mid 1990s, being in the early 2000s much warmer (~0.3 °C) and saltier (~0.06) than ~20 years ago. Only LIW and TDW were found at point C without any WMDW. As a probable consequence of the Eastern Mediterranean Transient, TDW was more of eastern origin than previously; but even more eastern TDW has been encountered since then. As illustrated by the figures in chapter 3, nowadays ranges for TDW at point C, which is the only time series commonly evidencing unmixed MWs, are 12.95-13.10 °C for θ and 38.48-38.51 for S, leading to σ ~29.10 kg.m^{-3}, which represents huge differences with GIB1,2 in the MWs ranges (see Fig.3b and 25e).

The CTD set at point M to monitor the inflow, in fact allows the monitoring of both the inflow and part of the outflow, due to the large amplitude of the internal tide (Millot, 2007). The inflow shows a marked seasonal variability of S (amplitude ~0.5, maximum in winter), due to air-sea interactions, and a huge ~0.05 yr^{-1} interannual salinification during the 2003-2007 period. Even though this result does not provide any information about the evolution of AW in the long term, it discredits all bulk analyses in the sea and at the strait that, more or less explicitly, assume a constant salt content within the sea. Note that, on some occasions (Fig.22b of M09), the MWs outflowing at point M (80 m) can de relatively dense, hence denser than the MWs outflowing at point C (270 m).

The CTD time series collected simultaneously (2004-2008) at points M, C and E (Millot and Garcia-Lafuente, 2011; MGL11 hereafter) provide information that fully supports all our previous results. Let us first note that both SAW and NACW are clearly recorded at M. The main result of MGL11 is to show that the outflow of MWs, which does not show a clear seasonal variability before entering the strait, strongly mixes within the strait, due mainly to the internal tide, with the seasonally variable inflow of AWs. The outflow thus gets marked seasonal and fortnightly variabilities within the strait. Furthermore, since the outflowing waters entering the strait display marked spatial heterogeneity and long-term temporal variabilities, while the inflow can display huge short-term variability, accurately predicting the characteristics of the outflow into the ocean appears almost impossible. More specific results of MGL11 are of special interest for the analysis herein and deserve to be detailed.

All the CTD profiles available in the MEDATLAS data base in the vicinity of the southern sills of Camarinal and Espartel show AWs-MWs mixing lines, but most of the profiles near the former sill also show more or less pure MWs near the bottom. This statistical feature inferred from data of unknown quality and large spreading in time is consistent with the high quality GIBEX data and suggests that linking the profiles with the time series can be roughly done by assuming that a given profile is displaced vertically by the internal tide, i.e. ignoring the advection and spatiotemporal variability of the mixing. Such an assumption is supported by the following analysis and the similarities between the spatial and temporal θ-S diagrams.

The MGL11 analysis is based on the mixing line slope computed from two successive records in a given time series (at t and t+1, "1" being the time step), more specifically on the ratio $(\theta_{t+1}-\theta_t)/(S_{t+1}-S_t) = \Delta\theta/\Delta S$, the unit of which is °C. Note that this is also the formulation of the mixing line slope computed from two successive data in a vertical profile, just replacing t by z. Practically, all θ-S diagrams herein are displayed with axes having the same length for a ΔS range that is half the Δθ one in classical θ (°C) and S units, so that the related slope $A=\mathrm{atan}(\Delta\theta/\Delta S/2)$ in degrees (°), computed and plotted in chapter 3, can be easily interpreted (the slopes in ° and in °C have the same numerical value). It also appears that 25-h median values of the slope efficiently filter out the diurnal and semi-diurnal tidal variability (and higher frequencies as well).

Most of the slopes (parameter A) of the AWs-MWs mixing lines, at the two sills and on the shelf of Morocco as well, were in the range -20° to -40° during the four-year period. More specifically, nearly all slopes at E are concentrated in that range, being there similar to the slopes at C and M, while positive slopes were also observed at C and M. These two negative values of the slope are figured out in Fig.3b and they were generally observed in the whole strait during GIB1,2, as shown by the θ-S diagrams in chapter 2; however, larger negative slopes can be observed, as during LYNCH (Fig.3a). One essential feature that will be illustrated herein is that points C and E are "luckily" (sic) located generally along the same streamline for the outflow, so that the along-stream evolution of the MWs outflowing there can be monitored (this is not the case for EN, see chapter 3.2).

All sets of slopes (at C, E and M) display a marked seasonal variability with, schematically, larger slopes (near -40°) in winter and lower slopes (near -20°) in summer. More specific features at C and E are schematized in Fig.3b, obviously in data ranges that are not those encountered nowadays. For instance, when the mixing line associated with two successive records in the time series at C is represented by the small-dashed lines near S=38.4, it is represented by the large-dashed lines near S=38.3 at E. This clearly indicates that a) when a MW at C mixes with a AW, that MW generally continues mixing with that AW at E, b) the MWs mix with two different AWs on a seasonal basis, and c) representative mixing lines associated with slopes of either -20° or -40° intersect in the MWs' range. An unmixed MW, schematized by the black circle in the TDW range, arriving at the sill of Camarinal will thus be modified, in the sill surroundings and depending on the season, towards values directed in a sector (-20°,-40°) all along its course westwards. And specifying a θ-S mixing line near C allows specifying the θ and S values expected at E (and vice-versa too), which provides a link between, for instance, CTD profiles near C and CTD profiles near E!

The negative slopes at M display a seasonality that is similar to those at both C and E, which accounts for AWs-MWs mixing processes occurring similarly over the whole strait. Very interestingly, slopes on the shelf are more negative than at both sills during the whole four-year period. Even though temporal θ-S diagrams at the sills do not show evidence of any relatively unmixed AW, the temporal diagram on the shelf and the spatial diagrams in the central part of the strait (e.g. Fig.16B of M09) indicate that the lowest (largest) slopes correspond to mixing of the MWs with some kind of NACW (SAW). The fact that NACW is deeper than SAW explains why the MWs on the shelf mix more with SAW than the MWs do in the deeper part of the strait. According to the GIBEX data (M09; hereafter), NACW can be either totally absent or concentrated near some specific latitude within the strait on time scales that can be as short as a few days. It can thus be concluded that the mixing of each of the MWs with the AWs occurs on time scales ranging from days to seasons (in the long-term as well) and is dependent on both the spatial distributions of NACW and SAW and on the cross-strait location.

Positive slopes in the range +55° to +75° are observed at C and M, not at E. At C, these slopes indicate mixing between pure MWs and the fact that mainly TDW has been outflowing there at that time (a +75° slope is schematized in Fig.3b), which is consistent with the fact that pure MWs can be found in significant amounts only at the sill of Camarinal and neither on the shelf of Morocco (M09) nor at the sill of Espartel (Garcia-Lafuente et al., 2007). At M, these slopes indicate mixing between NACW and SAW (data are too scarce in the MWs ranges), hence some kind of relatively pure AW (involving no MWs at all) associated either with the seasonal mixed layer or with wintertime mixing; such a slope could have been schematized in Fig.3a but can easily be imagined.

Additionally, the GIBEX data show (auxiliary figures 1, 2 and 3 of Millot, 2008) noticeable seasonal variability of the AW stratification down to relatively large depths (100-200 m) consistent with the seasonal variability of the positive slopes on the shelf of Morocco. Therefore, the whole outflow's characteristics, i.e. not only in its upper part but also down to the sills' depths, are dependent on the seasonality of the AW composition and stratification. It can be that, during summer, the seasonal pycnocline prevents AW in the mixed layer (i.e. SAW) from mixing with the MWs that consequently mix with relatively pure NACW (when present), i.e. with a relatively cool and fresh type of AW (slopes of ~-20°). During winter, the seasonal mixed layer disappears and NACW (when present) mixes with SAW so that, in any case, the MWs mix with a type of AW warmer and saltier than NACW that is some kind of SAW (slopes of ~-40°).

2. The water masses during GIBEX

When analyzing hydrographic transects so different in both north-south extent (4 to 70 nm) and maximum depth (300 to 1400 m), one must keep in mind the areas these transects actually represent as well as the consequences for both the outflow and the inflow. For instance, both flows having similar transports through the 4°30'W transect (90 nm, 1400 m) and the 5°45'W one (20 nm, 300 m), which has an area about 30 times less, their distribution and speed necessarily vary markedly from one transect to the other. Figure 4 allows comparing the various transects and giving an overview of the GIB1 and GIB2 data; even thought it was already shown in M09, it now displays a more accurate bathymetry. These actual bathymetric transects are used thereafter, instead of those inferred by M09 from the depth information reported in the header of the CTD profiles, to show the density sections. Since the data set and the bathymetry along these transects at nominal longitudes do not necessarily match, a drawback is that the data set cannot be fully represented, which gives us the occasion to remind the reader that satellite navigation systems in 1985-1986 gave only a few positions per day; however, longitudes reported in the headers were not exactly at nominal longitudes. Whatever the case, this does not change significantly any of the results herein.

Also plotted in Fig.4 are the AWs-MWs interface in red and a specific isopycnal in blue that is σ=29.08 kg.m^{-3} for all transects up to 5°40'W, expected to represent the light-intermediate / dense-deep MWs interface and used in the computations of M09, and other isopycnals in cyan west of 5°40'W, expected to schematize the stratification of the MWs outflow. Even though we previously argued for the changes we made in the definition of these various isopycnals, we must stress that their definition does not markedly change any of our results.

M09 wanted to show that some features always vary similarly as a function of the longitude so that both GIB1 and GIB2 were analyzed simultaneously. We now want to follow the various MWs and AWs from one transect to the other during each campaign, so that we analyze them separately; furthermore Fig.4 shows that the AWs-MWs interface was markedly different during both campaigns, in the Alboran subbasin in particular. We do this from east to west, since we are mainly concerned by the MWs, with θ-S diagrams similar to those in Fig.3a,b (i.e. one for the AWs and one for the MWs) and with the σ section. All available data are plotted in the θ-S diagrams with yellow dots, and one out of four (to provide visible information and up to 6°05'W) is numbered, according to the profile it represents, and coloured, according to the definitions we made in the Introduction; also specified with black numbers are the less-dense (densest) data in the AWs (MWs) θ-S diagram. As previously specified, all diagrams are displayed with axes having the same length for a ΔS range that is half the $\Delta\theta$ one in classical θ (°C) and S units; they cover the same ranges everywhere for the AWs and east of 5°50'W for the MWs, specific ranges being then used at 6°05'W and 6°15'W. All text information (names of the water masses, isopycnal values) in the θ-S diagrams having similar ranges are specified at the same place, thus allowing easier comparisons between them. All σ sections are displayed with a similar scale: the length of 0.1 unit (100 m) on the y axis equals the length of 0.1 unit (0.1 degree of latitude = 6 nm ~11 km) on the x axis. They are coloured according to the definition made in the Introduction using vertical lines in between two profiles when the MWs change from one profile to the other in a given σ range. Non-obvious isopycnals are specified in the figures captions.

2.1 During GIB1

Before analyzing the various transects, let us provide with Fig.5 an overview of the AWs and MWs characteristics in the 100-m surface layer with the distribution of S. Colouring of the arrows associated with the AWs is very schematic in the westernmost part of the area since NACW (green) is always found there at 100-200 m below SAW (cyan). In the strait, and even though NACW can be identified here and there, as well as in the sea, all mixing lines between the AWs and the MWs resemble that of profile 4 in Fig.3a (see below) and are thus coloured in cyan, so that the arrows schematizing (at 5 m) the circulation of the whole AWs layer are also in cyan. GIB1 is characterized in the Alboran by a huge north-south S gradient and a AWs-MWs interface intersecting the surface in the middle of the subbasin (Fig.4). This is a classical situation associated with an upwelling of MWs along the northern slope, generally of WIW (orange). Such a situation is also classically associated with an anticyclonic circulation (the so-called "western Alboran gyre") evidenced at the surface by the S=38.4 isohaline and at depth by maximum S values near 35.6°N-5°W and a bump in the AWs-MWs interface (Fig.4). In this area and as schematized at 100 m, the sluggish circulation of TDW (magenta) is inferred from the σ sections analyzed here below but, in the north, the homogeneous distribution of the S values associated with WIW indicates that this MW circulates significantly. Of specific interest are the large along-strait gradient at 50-100 m between 5°40'W and 5°30'W and the main location of the AWs in the northern part of the strait. The overall situation will be markedly different during GIB2.

At 4°30'W (Fig.6), the AWs layer is, as for all the other sections of this March-April campaign, relatively homogeneous, and it is relatively thin in the northern half of the section while it is bumped in the southern half due to the anticyclonic gyre previously described. The WIW core is well defined by profiles (p) 8 and 9 and still identified by p7 while p6-p3 only show mixed WIW. The LIW core has relatively similar properties at p7-p4 and only p3 shows LIW somehow mixed with TDW (at similar depths such as at p2). Neither WIW nor LIW can be identified at p1-p2. TDW is evidenced by all deep profiles; but while it is unmixed with the AWs at p7-p3, p1-p2 clearly show significant mixing between TDW and the AWs. WMDW is evidenced at relatively large depths (below 700-800 m) by all deep profiles (p3-p6) with a tendency to reach shallower depths southward (up to 500 m at p2). North of p5, the stratification is the one expected with intermediate MWs (WIW, LIW, TDWi) circulating significantly alongslope counterclockwise/westward. South of p5 down to ~500 m, the stratification is the one expected as a consequence of the gyre. The WMDW is distributed as expected from the circulation of the intermediate MWs.

At 5°00'W (Fig.7) previously described features are reinforced. The AWs layer is relatively homogeneous, it forms a bump centred on p3 and it does not spread northward at p5-p7 where WIW is found at the surface. The WIW core is found at p6 and also p5 while, at p4, it is relatively mixed with either the AWs or TDW at similar depths such as at p3.The LIW core is described by p4-p5 and not reached by p6. TDW is unmixed with the AWs at p4-p5 but still displays significant mixing with the AWs at p2-p3 (and p1 too). In the northern half of the section, the stratification down to the WMDW layer is the one expected for the general circulation of a relatively large amount of intermediate MWs while, in the southern half of the section, it is the one expected as a consequence of the gyre.

At 5°15'W (Fig.8) and even though the bathymetric section is more reduced than the 5°00'W one, similar features can be described. The layer of relatively homogeneous AWs does not spread far northward from p6, the core of WIW is sampled at p7-p9 and WIW can still be identified at p6 while relatively similar values define LIW at p6-p8. TDW, which occupies a relatively large percentage of the section, is unmixed with the AWs at p6-p7 only, but it appears to always mix with them, although in different ways hence not very intensively, at p1-p5. WMDW is only found in the deepest part of the southernmost deep profiles. Here also, the stratification is the one expected with a circulation of the intermediate MWs in the north and a AWs gyre in the south.

At 5°30'W (Fig.9), the situation is markedly different for both the AWs and the MWs. In the AWs layer, we are now upstream from the gyre, some stratification exists and one notes the occurrence of some NACW in the north. In the MWs layer, the TDW relative amount has markedly reduced. WIW is still well identified by its core at p4-p5, it is a bit mixed at p3 and much mixed at p2, being absent at p1 only. The same can be said for LIW, with similar core properties at p2-p4, mixed values at p5 (on the shoreward side of the core) and absence at p1 only. Even though TDW is found unmixed with the AWs at p2-p4 and relatively mixed with them at p1, it represents a relatively low percentage of the section area, while WMDW is still found in the deeper part of the section and mainly on the southern side of it. The stratification is the one expected for intermediate MWs circulating significantly and isopycnals sloping up southward.

At 5°40'W (Fig.10), features are similar, although more marked than at 5°30'W. The AWs layer is stratified and NACW can be evidenced at p5; note the relatively flat and even sloping up southward of the AWs-MWs interface, which is linked with the main location of the AWs in the northern part of the strait (Fig.5) and seems to be a rather uncommon situation. As already expected from the overall features (Fig.5), mixing has markedly increased in the 100-m surface layer at least, obviously below too, and WIW no more display a well-marked core. This is not the case of LIW that is still found relatively unmixed below WIW as is TDW at p4 only, complex interactions between LIW and TDW occurring at p3. Mixing of TDW with the AWs is now so huge that straight mixing lines are observed at p1-p2 in the whole MWs layer, as schematized in Fig.3b. The plotted mixing line is the best linear fit for all values from a given profile or set of profiles (here p1+p2) between the AWs-MWs interface down to the deepest part of the profile(s); it will be plotted on the θ-S diagram of the next transect as a dashed line ranging from the less mixed values on this present transect to the less mixed values of that next transect (and so on for the other sections). WMW clearly did not reach depths of 600 m there. The stratification is marked by the tilting up southward of the deep isopycnals associated with the circulation of the intermediate MWs.

At 5°50'W (Fig.11), first note the relatively regular stratification of the AWs layer as well as the occurrence of NACW at p6-p7, i.e. in the north of the section. The θ-S diagrams have dramatically changed in the MWs layer since all profiles display relatively straight mixing lines, which is a classical consequence of the huge mixing occurring since the surrounding of the Camarinal sills (5°45'W). Let us first start with p1-2 as their deepest values appear to be located just on the mixing line expected from p1-p2 at 5°40'W: for sure, p1-p2 at 5°50'W thus evidence TDW. Profiles 3, 4 and 5 at 5°50'W can just be expected to represent LIW, but a mixing line can be computed from p3. Similar features can be said for WIW and p6-p7, with a mixing line inferred from both profiles. To be noticed is that all the mixing lines defined at 5°50'W are computed from points that are roughly in line up to the AWs-MWs interface, and thus represent direct mixing between the AWs and each of the MWs. To be noticed also is that all these mixing lines have different slopes, which implies mixing with different AWs that is clearly evidenced by the θ-S diagram for the AWs in the range σ>28.0 kg.m^{-3}. Whatever the case, the MWs are objectively differentiated and juxtaposed.

At 6°05'W (Fig.12), the AWs layer is still markedly stratified, with still the occurrence of NACW, but now mainly in the south of the section. In the MWs layer, the two magenta dashed lines are those inferred from the mixings at 5°40'W (large dashes) and 5°50'W (small dashes) and they support the fact that p1 mainly evidences TDW. The deeper part of p2 could be on either the magenta or the red mixing lines inferred from the 5°50'W profiles p1-p2 and p3, respectively, but its upper part indicates it is more probably mixed LIW. The deepest part of p4 is exactly on the mixing line inferred from p6-p7 at 5°50'W and must therefore be associated with the same MW (we supposed to be WIW). Note that mixing lines either computed or displayed in the densest part of the AWs θ-S diagram are relatively similar: even though the upper part of the AWs layer display heterogeneities, its lower part displays relatively similar θ and S values. Here also, and whatever the case, the MWs are objectively differentiated and juxtaposed, with a tendency to be on the northern side of the section.

At 6°15'W (Fig.13), all profiles clearly evidence NACW and none of the AWs-MWs mixing lines directly involves SAW, which must be considered as an actual surface layer no more in contact with the MWs. In the MWs layer, profiles are radically different from the two previous sections since they clearly display undulations. Starting from p3, the densest values are exactly the same as the densest values of p1 at 6°05'W: the mixing line inferred from p1 at 6°05'W is thus useless and we are sure that the same MW (TDW) is identified by the two profiles. Mixing lines inferred from p2-p3 (associated with LIW) and p4 (associated with WIW) at 6°05'W are nearly similar in the range of interest at 6°15'W. We can first notice that both mixing lines are roughly aligned with the data at p4 and, second, consider that the differences between the p2-p3 and p4 densest values at 6°05'W (roughly 0.2 in S and 0.1 °C in θ) should be roughly maintained at 6°15'W so that, linking there the densest values at p4 with the densest values at 6°05'W (those we associated with LIW), one should retrieve with similar differences the less dense values at 6°05'W (those we associated with WIW). We thus come to associate these less dense values with the first undulation in the profile, and locate, at p4, WIW above LIW; coherently (following isopycnals), we then come to associate the undulations at p3 with WIW and LIW too, and we come with a stratification now showing superimposed (i.e. no more juxtaposed) MWs. The MWs are now clearly concentrated along the northern slope, where they will continue flowing while cascading. To be noticed also is the relatively large density gradient between WIW and NACW (all data are numbered).

2.2 During GIB2

The overview of the AWs and MWs characteristics in the 100-m surface layer provided by Fig.14 dramatically differs from that encountered during GIB1. While similar remarks can be made about the relative distribution of NACW and SAW in the westernmost part of the area, the flow of AWs then spreads smoothly in the whole Alboran subbasin where the dynamical relief is relatively flat (Fig.4) and no structure can be specified with the S distribution over a significant depth range. The circulation of both WMDW (blue) and WIW, at least at these relatively shallow depths, can only be inferred from the σ-sections. Also very different is the situation in the strait where gradients are no more along-strait but markedly cross-strait, especially large at 5°40'W, with the AWs mainly located in the south.

At 4°30'W (Fig.15), one first notes the marked stratification of the AWs layer that is characteristic of the September-October period, and the relatively flat dynamical relief expected from Fig.14. The distribution of WIW is relatively strange, although coherent since retrieved at 5°00'W: even though the WIW core, which is not reached by p7, is clearly sampled at p6, similar values are also observed at p3 (and p4 to a lesser extent) in the σ-range 28.95-29.00 kg.m^{-3}, but not at all at p5 in between, while, for σ<28.95 kg.m^{-3} the p3 values rapidly resemble the p5 ones. Such a "branching" on both sides of p5 is retrieved in the upper part of the LIW layer while the LIW core is homogeneous at p3-p6. TDW appears as a very homogeneous relatively thin (200 m) and flat layer while WMDW occupies the deeper part (>700 m) of the section and is markedly uplifted (up to 200 m) in the south where it clearly mixes with the AWs at p2. The stratification is the one expected with AWs spreading across the whole subbasin, and intermediate MWs that circulate without modifying the deep isopycnals.

At 5°00'W (Fig.16), similar remarks can be made about the AWs layer. The WIW core, not reached at p7, is clearly sampled at p6 and one can note that values at p5 tend towards the core values in the σ-range 28.975-29.00 kg.m^{-3}, but do not evidence WIW for σ<28.9 kg.m^{-3} (like the p3 values at 4°30'W). The LIW core is well defined at p5 while not reached at p6. Note that complex, and probably rare, interactions occur at p4 at ranges coloured in red and magenta with the mixed WMDW found at similar levels at p3 (so that the coloration is relatively complex and not necessarily accurate). TDW unmixed with the AWs is found only at p5 while WMDW unmixed with the AWs is found at p2-p5, significant mixing with the AWs being evidenced at p1-p4. The stratification is the one expected with AWs still spreading across the whole subbasin, and a relatively low amount of intermediate MWs that modifies the distribution of WMDW in the deeper part of the section and allows it to be the sole MW encountered in the southern half of the section.

At 5°15'W (Fig.17) the AWs layer is still markedly stratified, although relatively heterogeneous horizontally, and the dynamical relief is still relatively flat. In the MWs layer, the contrast is striking between p9 and mainly p8 that evidence a classical (like the one in Fig.3b) θ-S diagram and p1-p7 that all evidence significant mixing between WMDW and the AWs. The area occupied by the intermediate MWs is markedly smaller than that occupied by WMDW. The stratification in the MWs layer is only dependent on their westward circulation.

At 5°30'W (Fig. 18), the AWs layer is relatively thick and the AWs-MWs interface starts sloping up northward. The distribution of the MWs is relatively complex with WIW core values encountered more at p3 and p5 than at p4, a LIW core well defined only at p3 and complex mixing lines with the waters above at p2 and p4. In the southern part of the section (p1), one notes the relatively straight mixing line between WMDW and the AWs. The relatively reduced area occupied by the intermediate MWs and the relatively heterogeneous structure of the associated θ-S diagrams supports the occurrence of a relatively low amount of intermediate MWs as compared to that of the deep MWs. Whatever the case, isopycnal in the MWs layer are sloping up southward.

At 5°40'W (Fig.19), the AWs-MWs interface is clearly sloping up northward, consistently with the AWs main location in the south (Fig.14). WIW core values are mainly found at p4-p5 but also at p6. LIW core values can hardly be defined at p3-p5 and, even though there is nearly no trace of WIW there, no straight mixing line with the AWs can be defined. Even though TDW appears as a relatively thin layer, a mixing line can be computed in the upper part of p2. In the south, the WMDW amount is relatively important and a mixing line can be defined at p1. Even though defining core properties of the various MWs appears difficult, marked interactions with the AWs have started while isopycnals are markedly sloping up southward.

At 5°50'W (Fig.20), the θ-S diagrams in the AWs layer are markedly different with a more or less large influence of NACW that is clearly found at p1-p2. The AWs-MWs interface is markedly sloping up northward. In the MWs layer, the distribution of the various θ-S diagrams is relatively complex but can be logically specified using the mixing lines defined at 5°40'W. The lower part of p6 being clearly on the mixing line we associated with WIW allows coloring the p6 (and p7 too) profiles in orange while a new mixing line is defined from the p6 values. Similarly, the lower parts of p3 and p4 are on the mixing line we associated with TDW, so that they are coloured in magenta; but p3 and p4 values are not aligned enough and we cannot define a significant mixing line there. In between, we find at p5 two sets of values that are relatively different from those at p3-p4 and p6 while not being on the WIW mixing line. Because LIW was sampled at 5°40'W, we hypothesize it is found there and thus define two different mixing lines in the S-ranges 38.304-38.352 for the deepest one and 38.228-38.268 for the shallowest one. Characterization of the p1-p2 values is more obvious since densest values are on the mixing line associated with WMDW at 5°40'W. All four MWs are thus probably still evidenced at 5°50'W and juxtaposed.

At 6°05'W (Fig.21), the occurrence of NACW at p1-p3 and not at p4-p5 leads to very different mixing lines with the MWs while the AWs-MWs interface is relatively flat. No data are found on the mixing lines associated at 5°50'W with p6 (WIW) and the shallower part of p5 (LIW) but the deeper part of p4 can clearly be located on the mixing line inferred from the deeper part of p5 at 5°50'W and thus associated with LIW. Since the deeper parts of p3 and also p2 are clearly on the mixing line associated with WMDW at 5°50'W, they have for sure to be coloured in blue, as must also be p1 that obviously results from the mixing between "some already-modified-by-mixing WMDW" and NACW. Coherently with the relatively large amount of WMDW found in the Alboran, we thus come at the exit of the strait with still a relatively large amount of WMDW; however, having necessarily interacted with different AWs, it displays some heterogeneity. Also coherently with the relatively low amount of intermediate MWs in the Alboran, only one of them can still be evidenced at 6°05'W, which does not mean that the others cannot be evidenced; more probably, they were in too small quantity and the sampling was not dense enough.

At 6°15'W (Fig.22), NACW can be identified in the whole deeper part of the AWs layer so that SAW is clearly surface water there and no more interacts with the MWs that are sampled at only three profiles. Since the deeper part of p7 is clearly on the mixing line defined from p4 at 6°05'W and since that mixing line continues up to the AWs-MWs interface, it is clear that only LIW is found there. The deeper parts of p5 and p6 are on the mixing line inferred from p3 at 6°05'W so that they are associated with WMDW and coloured in blue. However, there are undulations at both p5 and p6 that tend toward the values at p7 and represent some modified form of LIW. We thus come with a stratification showing superimposed MWs that are clearly concentrated on the northern part of the section where they will continue flowing while cascading. Note the relatively large gradients between LIW and NACW on all profiles (all data are plotted).

3. The HYDROCHANGES / INGRES time series

While CTD time series are collected permanently at C, E and M (Fig.2) and have already given significant information (e.g. Millot et al., 2006; Millot, 2007; M09; MGL11), two additional time series were collected by the University of Malaga with another CTD deployed, in 2007-2008, successively at ES (during 128 days) and EN (during 64 days) that are roughly at the longitude of E. The original sampling interval is 0.5 h but we use here a 1-h sub sampling to compare the data at E, ES and EN with those at C. Correlations between the θ, S and σ time series at C and E (~21.2 km apart) during the 2004-2008 period all peak at a 8-h phase lag, which represents a realistic average flow speed of ~0.7 ms^{-1} (MGL11); all analyses and figures herein are thus made with a modified (-8 h) time at E, ES and EN. While E is just at the sill of Espartel (nominal depth = 360 m), both ES and EN are up on the slopes (nominal depths = 320 m) at 1.15 nm (2130 m) and 0.95 nm (1760 m), respectively, so that EN is slightly closer of E than ES is.

3.1 At the southern sill of Espartel (E) and south of it (ES)

To better understand the variability at all these places, let us first briefly describe the σ variability at C (Fig.23), which is the sole place where MWs unmixed with the AWs can be encountered, especially in favourable (neap tides) conditions. While unmixed MWs can be identified in the σ range 29.05-29.10 $kg.m^{-3}$, it is clear that spring tides intensively mix the MWs with the AWs; during this specific period, the minimum σ value reached at C was 27.7 $kg.m^{-3}$ (on day 31, d31). Such a fortnightly mixing also occurs at both E and ES (and EN too) with minimum σ values of 28.70 and 28.41 $kg.m^{-3}$ reached at E and ES, respectively, on the same day (d84) and even at the same time step, which validates the significance of such time series to study small scale phenomena. Whatever the case, it is important to note that the largest variations at both E and ES (and EN too) are due to the internal tide, which will not be so obvious when analyzing the filtered (25-h median, see MGL11) values thereafter. When comparing the raw data at E and ES in Fig.23, and apart from the fact that they display relatively similar variations, the main feature is that variations at ES are larger than at E, i.e. both largest and lowest densities are observed at ES.

Figure 24 shows the filtered data and parameter (θ, S, σ, A) at both E and ES. Before analyzing the variations displayed by these time series, let us first emphasize the fact that the fortnightly variability that was obvious in the raw time series (Fig.23) cannot practically be evidenced in the filtered ones, which might account for a relatively large variability in the characteristics of the MWs that were outflowing there at that time. Whatever, the slopes (parameter A) at both locations display nearly exactly the same variations, which will appear to be nearly exactly the same than at C too. The similarity of the slopes indicate that, at both places, the same MWs have mixed with the same AWs, both sets of waters varying with time since the slopes are markedly varying, roughly in the -20 to -40° range, at both E and ES (and C too) during the whole study period. All these general features are clearly displayed on the θ-S diagram in Fig.25a. Meanwhile, it is clear that all three data display similar variations that are larger at ES than at E, which provides important information that can be synthesized when dealing with σ.

First, the mean σ values inferred from the raw data sets are 28.955 $kg.m^{-3}$ at E and 28.950 $kg.m^{-3}$ at ES. When considering the maximum raw values of 29.058 $kg.m^{-3}$ at E and 29.071 $kg.m^{-3}$ at ES, which are thus clearly associated with relatively unmixed and dense MWs, and values of 28.85-28.90 $kg.m^{-3}$ (inferred from the filtered data sets in Fig. 24) that can be associated with relatively unmixed and light MWs, it can be assumed that mean values differing by only 0.005 $kg.m^{-3}$ for a data range of ~0.2 $kg.m^{-3}$ are practically the same. It can thus be assumed that, on average and during this experiment, both E and ES were located on the 28.955/28.950 $kg.m^{-3}$ isopycnal. Considering the differences in depth (360-320=40 m) and cross-slope location (2130 m), it can be concluded that this specific isopycnal has been sloping up southward with a slope of ~2%. Such a slope is fully consistent with those displayed at 5°50'W by the 28.97 $kg.m^{-3}$ isopycnal during GIB1 (Fig.11) and by the 29.01

kg.m^{-3} isopycnal during GIB2 (Fig.20), as well as with the slope (~3%) computed by M09 at 5°30'W-5°40'W from the GIBEX data. The direct measurements with the CTD time series at E and ES thus demonstrate what has been inferred from the CTD profiles: deep isopycnals in the strait are sloping up southwards (by 2-3%) so that densest MWs are located more along the southern Moroccan slope than at the sill (of Espartel south; the same is obviously expected for Camarinal south).

Values similar at both E and ES were encountered over the whole σ range and during the whole study period, so that a nominal 2% slope of the deep isopycnals is a common feature that illustrates the variability in the density and/or amount of the MWs outflowing there. It can also be deduced from these time series that the density at ES has been larger than the density at E during ~45% of the time, which clearly means that the slope of the deep isopycnals has been larger than a nominal value of 2% during 45 % of the time (i.e. lower than 2% during 55% of the time). Note that the ES data are more influenced by mixing with the AWs than the E data, since the latter are deeper, so that slopes larger than 2% only resulting from the outflow dynamics should occur more than 45% of the time. Considering, from the GIBEX data at 5°50'W (Fig.11, 20) as well as from all CTD sections near the southern sill of Espartel (shown in Fig.4a of MGL11) available in the MEDATLAS data base, that a classical value for the dσ/dz gradient there is (was in the 1980's?) 0.02 kg.m^{-3} for 100 m, we have tried inferring the deep isopycnals slope from the difference σ(E) –σ(ES) but did not get realistic results. Note that monitoring σ at two depths on each mooring would have allowed getting a time series of the deep isopycnals slope.

One can be easily convinced by Fig.24 that the MWs encountered at E and ES during this 128-day period were nearly the same; it is much less obvious to be convinced by Fig.23 that the MWs encountered at both E and ES were those encountered at C too! Whatever the case, this can be done considering the results of MGL11 schematized by the magenta mixing lines in Fig.3b: with the hypothesis that the mixing lines slopes (MLS) at e.g. E and C are the same, considering θ(E), S(E), MLS(E) and, for instance, S(C) allows computing a θinferred(C) that can be compared with θ(C), the temperature actually measured at C. Figure 26 shows that, even though the data θ and S, as well as the parameter MLS, were relatively different at E and C, θinferred(C) fits pretty well with θ(C). Results of similar quality are obtained during the whole 2004-2008 period (not shown). Even though θ(ES) and S(ES) were even more different from θ(C) and S(C), results of similar quality are obtained with ES (Fig.27). It might even be, considering |θinferred(C)-θ(C)|, that results obtained with ES are better than those obtained with E. This could simply be due to the fact that the streamline at C could be closer to the streamline at ES than to the streamline at E. The fact that the ES depth (320 m) is closer to the C depth (270 m) than the E depth (360 m) is not important since reducing the depth, as it is at Espartel, markedly increases the variability, hence leads to time series more different from the C ones where the variability (of filtered data) is nearly at a minimum.

The demonstration that the MWs at C, E and ES are nearly the same is made more obvious when considering the EN data.

3.2 At the southern sill of Espartel (E) and north of it (EN)

Figure 28 shows the filtered data and parameter (θ, S, σ, A) at both E and EN, the latter being 40 m shallower than the former (as for ES) and ~1760 m to the North only (ES was ~2130 m to the South). Before analyzing the variations displayed by these time series, let us first emphasize the fact that the fortnightly variability that is obvious in the raw time series (not shown since point C has been serviced during that period and data are not available to us yet,) can still be evidenced in the filtered ones, in particular E. This might account for MWs outflowing with relatively stable characteristics there and at that time, allowing the effect of the fortnightly mixing to be more clearly evidenced than during the period previously analyzed. Whatever the case, the three data sets and the parameter A as well display marked differences. All variables are in relatively different ranges and, although the fortnightly variability can be recognized at both locations, smaller scale variability at EN is much larger than at E. Parameter A is also significantly larger (i.e. less negative) at EN than at E (hence than at C) and it displays some variations not encountered at E. Before analyzing these differences, let us consider Fig.29 that displays the comparison between θinferred(C) and θ(C). Even though the comparison can be made during ~21 days only due to the C servicing, it is clear that the MWs outflowing at C were not those outflowing at EN (Fig.29a) while they were still those outflowing at E (Fig.29b), except during a short unusual event at the beginning of the period evidenced by MLS(E).

Now, to better understand the differences between the time series at E and EN displayed by Fig.28, let us first discuss the θ-S diagram in Fig.25b1,b2. At first sight, it could be that the warmer and fresher, hence less dense, MWs at EN result from the mixing with the AWs of those encountered at E. Such an analysis is obviously wrong since E and EN are located at the same longitude, i.e. in a direction perpendicular to the main outflow, so that they are located along different streamlines and MWs there have mixed with the AWs during roughly the same time since the Camarinal surroundings. Since both the MWs and the AWs have noticeably changed during the study period (as indicated by the variability in Fig.28), we have to wonder whether, at the same time, different MWs and/or AWs could have occurred at the two places. Mixing lines can provide definite answer according to three different situations: a) when a single MW is mixing with different AWs (at e.g. E and EN), mixing lines (at e.g. E and EN) intersect in that MW range (e.g. as specified at C or upstream); b) when a single AW is mixing with different MWs, mixing lines intersect in that AW range (e.g. as specified west from the strait); c) when different AWs are mixing with different MWs, mixing lines intersect "elsewhere". Focusing on this later situation, and considering the θ-S diagrams in the AWs and MWs ranges (e.g. Fig.3a,b), it is obvious that, if mixing involves SAW and LIW at one place while it involves NACW and WMDW at the other place, mixing lines will intersect out of the AWs-MWs range: this will be towards very fresh and warm (salty and cold) waters if the distance SAW-NACW is smaller (larger) than the distance LIW-WMDW. Now, if mixing involves SAW and WMDW at one place while it involves NACW and LIW at the other place, mixing lines will intersect within the AWs-MWs range in an area that has nothing to do with any of the waters considered individually.

We have thus computed the mixing lines inferred first from the unfiltered set of data and noticed (Fig.25c) that they intersect in a relatively large AWs-MWs range so that we definitively have to assume that both the AWs and the MWs at E and EN were different during that specific period. Considering filtered (median / 25 h) data and mixing lines (Fig.25d) shows that intersections clearly occur in between the data sets at E and EN, so that we obviously tried to specify if such a situation is possible or not, which is schematized in Fig.25e. We lack basic information that is "which were the MWs outflowing in the Camarinal surroundings during that specific period?" We thus have to rely on some standard profile and used the one at 4°30'W during GIB2 shown in Fig.3b that is plotted as black dots in Fig.25e; note that, apart from being relatively regular, thus explicit, it displays values similar to those at 5°40'W during either GIB1 (Fig.10) or GIB2 (Fig.19). We assume it could represent a standard profile in the Camarinal surroundings nowadays provided it is shifted to take into account the warming and salting of the MWs in the 2000's as compared to the 1980's (Millot et al., 2006). More accurately, we shifted the profile (red dots) so that the part corresponding to TDW (magenta in Fig.3b), which is the MW most frequently observed at C (see the θ-S diagrams in M09 and MGL11), has the θ and S values observed at C during the 64-day period, at least at its beginning, as indicated by Fig.29 (θ(C)=13.0-13.1 °C, S(C)=38.45-38.50, which are clearly values defining TDW, i.e. neither LIW nor WMDW). Then, we computed the average of the mixing lines slopes as indicated by parameter A (Fig.28) in the range 0 to -50° and got mean values for A of ~-25° at EN and -31° at E. We plotted these averaged mixing lines (as blue and cyan arrows in Fig.25e) so that they correspond to the center of mass of the data at EN and E, respectively, and got two major results: a) the mixing line at EN roughly corresponds to the LIW core at C while the mixing line at E clearly corresponds to the MW (i.e. TDW) simultaneously measured at C (θ=13.0-13.1 °C, S=38.45-38.50), and b) these two averaged mixing lines intersect in the brown dots area.

Considering the roughness of our hypotheses, in particular about the representativeness of the vertical profile at C during the 64-day period, we are conscious that Fig.25e cannot be a demonstration. But our interpretation, done as objectively as possible (i.e. using as much as possible the available data and parameters) must obviously be considered for further analyses. The most probable hypothesis able to explain the differences observed between the time series at E and EN is to assume that a mixture of LIW and a "more NACW-like" AW was outflowing at EN while a mixture of TDW and a "more SAW-like" AW was outflowing at E. This is obviously consistent with our general concept of MWs outflowing juxtaposed, i.e. side by side and the denser the more to the south, in particular in the Espartel surroundings!

4. Discussion

4.1 AWs vs. MWs heterogeneities

One point we never emphasized in any of our previous papers concerns the differences between the AWs and MWs heterogeneities in the study area that are directly linked to the forces driving them through the strait, hence to the functioning of the sea. The sea is a machine that basically transforms the AWs, the raw material, into the MWs, the product, using a unique source of energy that is the evaporation (or more exactly the E-P budget); all other parameters involved in the air-sea exchanges (latent and sensible heat transfers, wind stress, etc.) just modify the product, they do not run the machine.

Indeed, evaporation just makes the level of the sea lower than that of the ocean so that the AWs just enter the sea "to fill the hole, they are sucked, they cascade". Whatever the image, the major implication is that any AW flowing, according to this or that typically oceanic process, in the western surroundings of the strait can enter the strait from anywhere. Even though NACW is always denser than SAW, parts of it can thus be entrained in either the southern or northern part of the strait. Heterogeneity of the inflow within the strait will thus be somehow erratic. Then, because neither the SAW nor the NACW have specific dynamics there, they are rapidly mixed so that one deals with a unique AW in the sea.

On the contrary, the different MWs are formed in different areas of the sea every winter and hence have specific θ-S-σ characteristics that will allow recognizing them everywhere in the sea, the strait …and maybe the ocean too! They first accumulate in these areas before spreading and circulating more or les intensively as density currents, hence essentially alongslope counterclockwise. Each basin of the sea continuously forms, year after year, both intermediate and deep waters, and both types of waters necessarily have different ways to escape from that basin. While the intermediate waters can cross either the channel of Sardinia or the strait of Gibraltar while continuously circulating, the deep waters can't and first remain trapped within their basin of origin: they are then uplifted, year after year, by younger and denser waters up to overflowing through either the channel or the strait. Now, only because of the Coriolis effect, which makes all these waters circulating alongslope counterclockwise, as long as they are not either motionless or uplifted, the intermediate waters outflow essentially on the right hand side of either the channel of the strait; and only because they necessarily accelerate in such passages, the Coriolis effect intensifies so that the intermediate-deep MWs interface tilts up on the left-hand side of either the channel or the strait, up to lifting the deep MWs just below the AW. Both the intermediate and the deep MWs are thus pushed out of the sea according to very specific forces and processes that will lead them to occupy very specific positions within either the channel or the strait. Whatever the number of MWs outflowing through a given passage in sufficient amount to be identified, hence whatever the heterogeneity of the MWs outflow, it will remain structured and driven by specific forces, so that it will keep its heterogeneity while crossing the strait in particular.

4.2 The AWs overall characteristics

In the ocean (at 6°15'W; Fig. 13, 22), the AWs vs. MWs distributions are relatively similar. For the AWs, first note the homogeneity of the SAW layer during both campaigns, hence whatever the season. The amount of NACW vs. SAW is a bit larger during GIB1 but the NACW core, roughly indicated by the σ=27.0 kg.m^{-3} isopycnal is found at relatively similar immersions across the whole section. At 6°05'W (Fig. 12, 21), and even though the MWs amount seems to be a bit larger during GIB1, the distributions of NACW and SAW are relatively similar too with a relatively homogeneous SAW layer and NACW found only in the southern half of the section.

Within the strait at 5°50'W (Fig. 11, 20), the MWs amount is now clearly larger during GIB2 and the AWs-MWs interface, as defined by the σ=28.0 kg.m^{-3} isopycnal, is sloping up northward more clearly during GIB2 too; note that the AWs-MWs interface as defined by the S and σ vertical gradients is relatively similar during both campaigns. Whatever the case, SAW is les homogeneous than more to the west while NACW is encountered in the north during GIB1 and in the south during GIB2. At 5°40'W (Fig.10, 19), the AWs-MWs interface is horizontal or even sloping down northward during GIB1 while it is markedly sloping up during GIB2, which has to be associated with the large north-south gradient encountered in the AWs layer in the S distribution (Fig.14) as well as in the θ distribution at the surface. NACW is encountered only during GIB1 on one profile in the north of the section. These features are relatively consistent between both sections but will markedly change then.

In the eastern part of the strait (5°30'W, Fig.09, 18), features are relatively different for the AWs-MWs interface that indicates a larger amount of MWs during GIB1 and a sloping up northward across the whole section while the AWs amount is relatively large during GIB2 and the interface is sloping up northward only in the northern part of the section. Consistently with the two previous sections, NACW is found on all northern profiles during GIB1 and is absent from all profiles during GIB2. During GIB1, the differences between the 5°40'W and 5°30'W sections are linked with the strong east-west gradient on the S distribution in the AWs layer emphasized in Fig.05. More to the east (5°15'W, Fig.08, 17) the AWs-MWs interface features have reinforced since the interface is now markedly sloping up northward and even intersecting the surface during GIB1 while it is almost horizontal and relatively deep during

GIB2; during both campaigns, NACW and SAW are now well mixed. These features are significant since they will be consistent with the features in the Alboran subbasin.

Indeed, in the western part of the Alboran (5°00'W, Fig.07, 16), the AWs-MWs interface during GIB1 is still intersecting the surface and it clearly depicts a bump centred on p3 associated with the anticyclonic gyre while it is almost flat over the whole section during GIB2. At 4°30'W (Fig.06, 15), a thin AWs layer has spread northward while interacting with the MWs, but most of the layer, which has markedly different and more homogeneous characteristics, still depicts the anticyclonic gyre in the south. A relatively thick layer still spreads across the whole subbasin during GIB2.

When trying to get an overview of the AWs distribution, one is not too surprised by the similitude found between GIB1 and GIB2 in the ocean (6°15'W, 6°05'W) since the interactions with the MWs layer are limited there. Within the strait (5°50'W, 5°40'W), the relatively flat and deep AWs-MWs interface during GIB1 as compared with GIB2 suggests (erroneously!) a larger and relatively slow inflow during GIB1. But features markedly change in the eastern part of the strait (5°30'W, 5°15'W) since the AWs-MWs interface now comes to be shallower and more steeply during GIB1, hence suggesting (correctly!) a relatively small and rapid inflow during GIB1 that lead to well marked dynamical features in the Alboran (5°00'W, 4°30'W). However, since common sense would normally associate a rapid inflow with a large amount of AWs entering the sea, one would have expected more AWs in the Alboran during GIB1 than during GIB2. This simply illustrates how bad our present understanding of the sea-ocean exchanges is.

4.3 The MWs overall characteristics

At 4°30'W (Fig.06, 15), the WIW and LIW amounts are relatively similar and they extend relatively far to the south during both campaigns; because of the AWs amount, they are just deeper during GIB2. Over most of the section, the TDW and WMDW location and amount are relatively similar too but, off Morocco, TDW (WMDW) is found just below the AWs during GIB1 (GIB2). At 5°00'W (Fig.07, 16), both WIW and LIW extend southward as far as the middle part of the section only and WIW, found at the very surface during GIB1 also displays a larger amount than during GIB2. Below, while the TDW vs. WMDW distribution is relatively similar in the northern part of the section, TDW (WMDW) occupies the whole southern part during GIB1 (GIB2).

At 5°15'W (Fig.08, 17), features are similar than those at 5°00'W with WIW extending up to the very surface and both WIW and LIW in larger amounts during GIB1. TDW occupies most of the southern part of the section during GIB1, hence interacts markedly with the AWs while, during GIB2, TDW is indicated by p8 only and WMDW occupies the whole southern half of the section. At 5°30'W (Fig.09, 18), WIW has sunk below the AWs but the WIW and LIW amounts are still larger during GIB1. Both TDW and WMDW are flanked along the southern slope, TDW only interacting with the AWs and WMDW reaching only ~500 m during GIB1 while WMDW is interacting with the AWs during GIB2 and is thus juxtaposed with TDW.

At 5°40'W (Fig.10, 19), both WIW and LIW have continued sinking below the AWs and are thus deeper than during GIB2 but their amount are now roughly similar. WMDW is no more indicated during GIB1, so that TDW is found in the whole southern part of the section with isopycnals clearly sloping up southward. During GIB2, both WMDW and TDW are still outflowing side by side and even LIW is now interacting directly with the AWs. At 5°50'W (Fig.11, 20), WIW, LIW and TDW are outflowing side by side during GIB1; note that large amounts of TDW at p1-p2 are not clearly represented by the actual bathymetric profile. During GIB2 the four MWs are outflowing side by side and they represent a total amount seemingly larger than during GIB1.

At 6°05'W (Fig.12, 21), the part of the section occupied by the total outflow is larger during GIB1 than during GIB2. WIW, LIW and TDW are still identified and juxtaposed during GIB1 while only WMDW and LIW are identified and juxtaposed during GIB2. The same MWs have been identified at 6°15'W (Fig.13, 22) but features are much less obvious than more upstream. First, note that the MWs outflow is identified by the lower part of 2-3 profiles only. Then, identification of the MWs is made according to either mixing lines at 6°05'W for the MW that outflows on the bottom, or to undulations in the profiles for the MW that outflow above. Even though this is obviously what must be expected with MWs now superimposed, association between an undulation and a given MW cannot obviously be as clear as was the case upstream between a mixing line and a given MW. Even though we are more confident in the identification of the various MWs made herein than by M09, it must be emphasized that, due to the relatively low number of profiles and data, both remain markedly hypothetical.

When trying to get an overview of the MWs distribution, let us first emphasize that, much more than for the AWs, the already fine sampling is far from being sufficient. What can be noticed in the eastern part of the Alboran subbasin is that the immersion of the intermediate MWs is clearly dependent on the AWs thickness, assuming that the dynamics in the AWs layer and the formation of the western Alboran gyre are not a consequence of the MWs outflow! It can also be noticed that the relative importance of TDW vs. WMDW in the final outflow can be predicted according to which MW is found on the Moroccan side of the sections in the Alboran just below the AWs, since WMDW is always found there below 600-700 m.

WIW, which was at 0-200 m in the Alboran during GIB1 was constrained to a 100-200 m layer at the strait entrance while, being at 100-300 m in the Alboran during GIB2, it was found at 50-200 m when entering the strait; even though amounts are similar within the strait, WIW is not sampled west from it during GIB2. The LIW amount and immersion also displayed complex variations in the Alboran and it is only at the strait entrance that amount seem larger and immersion deeper during GIB1; it seems that the LIW amount within the strait and west of it are still larger during GIB1. TDW appears to be a major component of the outflow as soon as the eastern Alboran during GIB1 and will effectively be followed all across the strait; during GIB2, and even though it will represent only a minor component in the Alboran and at the strait entrance, it will still be identified within the strait and finally non sampled west of it. WMDW, which never entered the strait during GIB1, represented more than half of the section area in the western Alboran during GIB2 and was followed all across the strait then.

Even though the GIBEX data represented a huge effort to collect data of utmost quality, it is clear than sampling intervals, in both cross-strait and along-strait directions are not small enough to specify heterogeneities that were not expected at those times. Whatever the case, we are convinced that all four MWs can be followed from east to west, from the sea to the ocean, just considering density and temperature ranges where mixing with the AWs is relatively limited, and mixing lines where it is of major importance, as in the southern part of the sections in the Alboran subbasin and within the whole strait. Sampling interval will have to be especially fine in the western part of the strait, when the MWs come superimposed again since they no more mix with the AWs and mixing lines can no more be used.

4.4 Schematization of the AWs-MWs mixing processes

Figure 30 is a first attempt to schematize our understanding of the mixing processes between the AWs and the MWs in the study area. Due to the extremely large variability in i) the composition of both the AWs inflow and the MWs outflow, ii) the dynamics of the AWs inflow essentially, iii) the immersion and inclination of the AWs-MWs interface, one cannot be fully satisfied by such a schematization since actual features are far from being so simple; whatever the case, we have tried! The diagram from the ocean to the sea across the strait (Fig.30a) allows representing the AWs all along their course as well as all MWs in the strait and west from it; in the sea, the MWs general behaviour is schematized as if it were TDW (Fig.30a) while more detailed features are schematized for WIW and LIW (Fig.30b), as well as for WMDW (Fig.30c).

As schematized in Fig.30a, AWs unmixed with the MWs can be found from the ocean (in a 200-300 m surface layer in the west of the study area) up to the sill of Camarinal and even more to the east, as NACW till 5°30'W during GIB1 when the AWs-MWs interface was at 50-70 m; in the sea, NACW has never been identified but SAW has been found with characteristics similar to those it had in the ocean, as at 0-100 m during GIB2. In the east of the study area, most of the MWs are not markedly mixed with the AWs entering the sea, mainly because they have not been in contact yet since most of the MWs flow along the Spanish continental slope while most of the AWs flow along the Moroccan one. Their mixing with the AWs is still generally limited in the Alboran, but it intensifies when approaching the strait; whatever the case, at least those MWs outflowing at Camarinal sill south can outflow still unmixed with the AWs in the deeper part of the sill during neap tides. It is only west from Camarinal that the totality of all MWs comes to be mixed with the AWs, so that mixing lines there extend down to the bottom; obviously, and as demonstrated by all data sets, each of the MWs in particular and the MWs outflow in general never comes to be homogeneous. Other features we tried to schematize are: for the AWs, the relatively low mixing with the MWs when the latter cascade in the ocean, the important mixing between the sills of Espartel and Camarinal, the fact that, in the sea, the part of the inflow that has been mixed with the MWs then tends to become homogeneous again; for the MWs, the fact that, after the intense mixing encountered in the sills area, mixing with the AWs is relatively reduced and each MW more or less evolves independently, its densest/saltiest part found close to the bottom in the sills area having to become the core of a vein while cascading along the Iberian slope (see 4.5).

In the northern part of the Alboran subbasin (Fig.30b), the thickness of the AWs layer becomes relatively low, up to being absent as during GIB1, so that WIW can be found at the surface there. Necessarily, and this will be the case for all MWs while in the sea, WIW will sooner or later mix with AWs, but with AWs that have already been mixed with some MWs within the strait, never with unmixed AWs: stratification in the lower part of the AWs layer thus becomes relatively complex. Then, most of the time, WIW will encounter a AWs layer thicker and thicker, so that it will generally have to sink while mixing. Being the lightest, hence shallowest of the MWs, it will remain just below the AWs layer along the Spanish continental slope and will then outflow through Camarinal sill north and Espartel sill north (see Fig.2), i.e. it has practically no chance to be sampled at neither C nor E, even EN.

Things are markedly different for LIW that never came in contact with the AWs before 5°40'W (as was the case during GIB2 only); they are roughly similar for TDWi as well, although differentiating it from TDWd, which will be assimilated to WMDW, is relatively artificial. Whatever the case, LIW is found at 300-500 m in the Alboran, so that it has to flow up to the Camarinal sills and is indeed found at 200 (sometimes less)-400 m at 5°40'W during both GIB1 and GIB2. We have shown (chapter 3.2) that LIW could be encountered at EN, obviously in relatively mixed conditions, but not at E during a relatively short period of 128 days. Values that could be associated with unmixed LIW at Camarinal nowadays (θ~13.15 °C, S~38.51) have been sampled at C in 2003 (E was not operational yet) only, no more in 2004-2008 (Fig.22a of M09). Therefore, it might be that, most of the time, LIW outflows through Camarinal sill north (not C), part of it then outflowing in the northern part of Espartel sill south (typically at EN, not E), which would be roughly consistent with streamlines that could be inferred from e.g. Fig.2.

In the southern part of the Alboran subbasin (Fig.30c), features are practically opposed to those in the northern part. Except for the unmixed upper part of the AWs layer that can be expected to be roughly similar, even if a bit thicker, most of the layer deepens, just because it will be constrained along the African slope by the Coriolis effect. Note that it will then lead to the Algerian Current that is much deeper along the slope than the ~200 m schematized here and is markedly unstable (Millot, 1985); and note also that no intermediate MWs is outflowing there (Fig.2 of M09) so that the AWs are in direct contact with the deep/dense MWs, be they TDWd as during GIB1 or WMDW as during GIB2. These deep/dense MWs circulate only sluggishly westward, since they have to outflow from the sea, so that they will be in contact with the AWs for a relatively long time. Additionally, the mesoscale instabilities generated by the Algerian Current extend over the whole depth while having a complex two-layer structure, which will increase the AWs-MWs mixing, not considering the effect of the Alboran gyres. As demonstrated by the mixing lines depicted at 4°30'W by the southernmost profiles during both GIB1 (Fig.6) and GIB2 (Fig.15), the upper part of the dense/deep MWs represented by WMDW in Fig.30c are markedly mixed with the AWs much before the strait entrance. Whatever the case, and clearly due to the tilting up southward to the isopycnals before and within the strait that is i) clearly depicted by all GIBEX sections, ii) evidenced by the CTD time series at ES vs. E (chapter 3.1), iii) evidenced by the CTD time series at M vs. C (Fig.22b of M09), relatively unmixed dense/deep MWs can outflow through the strait. However, and even though we personally do not think necessary to invoke a Bernoulli suction argument to explain the presence of WMDW at Camarinal sill south (Stommel et al., 1973) and even further west (Kinder and Parrilla, 1987), data able to specify how deep in the Alboran subbasin were the densest MWs that are outflowing in the lower part of the Moroccan slope at Camarinal sill south (at a point that would be the counterpart of ES) are clearly lacking.

4.5 Schematization of the AWs inflow and MWs outflow

Because our most original hypotheses concern the MWs outflow, let us describe Figure 31 from east to west. We have drawn our diagrams assuming that all MWs have roughly similar transports.

In the western part of the Alboran subbasin (5°15'W), the three intermediate MWs, which are circulating along the Spanish slope one above the other, push the deep MW along the Moroccan one, with the intermediate-deep interface sloping up southward, hence being nearly parallel to the Moroccan slope. The deep MWs area is relatively large since WMDW circulates less rapidly than the other intermediate MWs. Only WIW in the north and WMDW in the south mix with SAW only since NACW can hardly be identified there.

At the entrance of the Strait of Gibraltar (5°40'W), the available section dramatically reduces so that the intermediate MWs accelerate and increase both the interfaces between each other and the interface with the deep MW. We drew all interfaces intersecting at one singular point to show how variable the situation here can be, with LIW and/or TDW mixing for the first time with the AWs. Note that NACW can sometimes be still identified here.

From the Camarinal section to 5°50'W and to the Espartel section, all MWs are juxtaposed and mix with SAW and/or NACW. Since this mixing is mainly due to the internal tide while the AWs display a marked seasonal variability (MGL11) and variability (SAW vs. NACW) on a daily-weekly time scale that can be huge (Millot, 2008), it is there that all components of the MWs outflow mainly acquire the characteristics they will have in the ocean.

At the exit of the Strait of Gibraltar (6°15'W) the available section widens so that the MWs outflow starts flowing as a density current, hence accumulating along the right-hand slope. All MWs circulate independently while cascading one above the other and mixing only with NACW. Along the Iberian slope more to the north, the MWs form independent veins, the θ-S-σ characteristics of which can hardly be predicted with the accuracy foreseen up to now.

5. Conclusion

Our original ideas about the strait of Gibraltar are in fact relatively old since, even though not made especially explicit, they are underlying in all the papers we wrote about the circulation in the western basin (e.g. Millot, 1987, 1999) and in the whole sea (Millot and Taupier-Letage, 2005) that seem to be widely accepted nowadays (Schroeder et all, in press). During GIBEX (1985-1986) and the next decade, we were involving ourselves in the study of the Algerian subbasin, but we participated in the most important meetings dedicated to the strait functioning and got the feeling that processes could be markedly different from what was generally assumed at that time. When we initiated the HYDROCHANGES Programme, we emphasized the importance of monitoring the AWs inflow (Millot and Briand, 2002) and, thanks to the kindness, motivation and efficiency of just a few persons at SHOMAR, we deployed the first CTDs at points M and C in early 2003. We used ships that were not equipped for such kind of operations but all the SHOMAR personnel were willing to do their best and were actually very efficient since we serviced both CTDs fifteen months after.

These first records were too short to give significant results at M but they clearly evidenced at C dramatic changes in the MWs outflow that was much warmer (~0.3 °C) and saltier (~0.06) than ~20 years ago. Presentation of these preliminary results at the HYDROCHANGES Round Table held during the 2004 CIESM Congress in Barcelona had to face a quasi general marked scepticism, clearly confirming how difficult presenting new ideas is. Anyway, we were soon able to support these long-term changes by complementary data and to propose our first schematic diagram of the MWs outflow structure (Millot et al., 2006). Meanwhile, the SHOMAR efficiently helped us in regularly servicing the CTDs, allowing us to evidence some major aspects of the AWs variability. We demonstrated that the inflow shows a marked seasonal variability of S (amplitude ~0.5, maximum in winter), due to air-sea interactions, and displayed a huge ~0.05 yr^{-1} interannual salinification during the 2003-2007 period (Millot, 2007). We also started re-analyzing the GIBEX data (LYNCH campaigns) and evidenced a huge 10-day (or even less) variability in the inflow composition leading, through tidal mixing, to a huge few-day variability in the outflow characteristics (Millot, 2008).

We then started comparing the C and M time series and performing a detailed re-analysis of the GIBEX data (in particular the GIB1 and GIB2 campaigns) that are still nowadays extremely valuable since the studied area has no more been sampled with such small sampling intervals in both space and time. Both data sets have allowed us (Millot, 2009) supporting the hypotheses about the structure of the MWs outflow that we clearly formulated for the first time in our 2006 paper. We have then been able to compare the time series collected simultaneously during about four years at C, M and E, and evidenced the marked seasonal variability that the outflow gets while mixing with the inflow in the strait, namely since the Camarinal surroundings as we are convinced that it cannot display any seasonality before entering the strait (Millot and Garcia-Lafuente, 2011). However, our ideas still having to face a general scepticism since, for instance, only LIW and WMDW are still generally assumed to outflow at Gibraltar, we decided to make an analysis as objective as possible of the distribution of the in- and out-flows overall characteristics. When trying to objectively specify the characteristics of each of the AWs and MWs, we realized that associating the θ relative maximum and the S absolute maximum with LIW probably resulted from and astounding general misunderstanding (Millot, submitted). All these results constitute the background of the analysis herein.

A first point emphasized by Fig.2 is that both Camarinal and Espartel sections have two sills and that only the southern ones are monitored with CTD time series, which prevents from monitoring the lightest part of the MWs outflow. Figure 3a emphasizes how large is the variability in the structure of the AWs layer (σ<28.0 kg.m^{-3}) in the western part of the strait and how dramatic are the consequences for the outflow characteristics (σ>28.0 kg.m^{-3}); it is supported by all θ-S diagrams for the AWs at each sections in Fig.6-13 and 15-22. The θ-S diagram in Fig.3b, and all those for the MWs at each sections in the eastern part of the strait (Fig.6-9 and 15-18) as well, are similar to those found in most of the western basin (see Fig.2 of Millot, submitted), thus indicating that all major MWs (WIW, LIW, TDW and WMDW, i.e. not only LIW and WMDW) can clearly be identified in the outflow. As schematized in Fig.3b and illustrated by the θ-S diagrams in the strait (in particular Fig.10-12 and 19-21), straight mixing lines between the AWs and the MWs can be observed over the whole depth and can involve any of the MWs. Due to the overall winding shape of the θ-S diagrams in the MWs range, one consequence is that a given set of θ-S-σ characteristics cannot be directly associated with a given MW and that a specific analysis of each individual CTD profile has to be made.

We then proposed an as objective as possible differentiation of the AWs and MWs components based, for the AWs, on density ranges and the possible occurrence of a θ minimum since a S minimum has always been encountered during GIB1-2, which is not the general case as evidenced by the LYNCH profiles. For the MWs, and where they are not mixed yet with the AWs, the differentiation we propose is based on density and temperature ranges that can be modified according to one's personal choices. Where θ-S diagrams display a relatively straight shape, be it adequate for defining mixing lines or not, our differentiation just consider the MW involved in the deepest part of the profile. Whatever the names/colours given to these different ranges, and furthermore mixing lines generally allow linking data collected along successive sections/longitudes (Millot and Garcia-Lafuente, 2011), such an objective differentiation provide consistent and realistic results, at least up to the western end of the strait (as demonstrated by the σ sections in Fig.6-12 and 15-21). Then (Fig.13 and 22), available profiles (2-3 per section) are clearly not sufficient to differentiate the four MWs expected to outflow there.

Whatever the case, we understand that the re-analysis of the GIBEX data we made can be still not convincing enough, even though we are unable to find any feature inconsistent with our general overviews of the dynamical processes in the strait. Now, the HYDROCHANGES/INGRES time series collected by the University of Malaga at E, EN and ES provide information that cannot be discussed and must be integrated in any analysis of the Strait of Gibraltar functioning. Mean densities at E (360 m) and ES (320 m) are nearly the same, hence supporting the mean sloping up southward of the deep isopycnals. Densities at ES are often larger than at E, supporting the banking of the densest MWs along the Moroccan slope. Retrieving the characteristics at C from those at E, and even more efficiently those at ES, support our own understanding of the mixing processes within the strait and the fact that all three locations are, in general, roughly located along the same streamlines. The marked differences between the E and EN time series (closer to each others than E and ES), and the inability of the EN data to allow retrieving the C ones, clearly account for the fact that a different (and lighter) MW has been outflowing at EN only. Even though we had to make relatively strong hypotheses, what we did as objectively as possible, our results clearly suggest that TDW was outflowing at both C and E while LIW was outflowing at EN.

Whatever the reticence of our colleagues to accept our hypotheses, we are thus very confident in the assumption that the complementary data we plan to collect in the future, as well as the numerical simulations we hope will be made soon will support the data analysis and rough computations we have been able to make up to now.

Acknowledgements: This paper is a contribution to the CIESM HYDROCHANGES Programme (ciesm.org/marine/programs/hydrochanges.htm) and to the Spanish-funded INGRES projects. I warmly thank Frédéric Briand and the CIESM for their constant support, as well as Bernard Tramier from Total-Elf and the Bonus-Qualité-Recherche service of the Université de la Méditerranée who provided funds that have allowed me initiating the HYDROCHANGES Programme. I also warmly thank the CNRS (Centre National de la Recherche Scientifique) and the successive Directors of the LOPB (Laboratoire d'Océanographie Physique Biogéochimique) for providing me with almost exceptional working conditions. I will never forget the kindness, enthusiasm and efficiency manifested by Youssef Tber who succeeded in involving the SHOMAR in sea operations that were far from being a priority for such an organism and who made possible all the important results we got up to now. I thank Jean-Luc Fuda for having helped me conducting the first sea operations there and then, together with Gilles Rougier, Isabelle Taupier-Letage and Patrick Raimbault, for having managed with instrumental, logistic and diplomatic problems to continue the HYDROCHANGES programme in such a strategic place. I also thank Jesus Garcia-Lafuente for having allowed me, with the kind help of Antonio Sanchez-Roman, using his Espartel time-series and bathymetric data set. I finally thank the crew of S/Y "Ailes et Iles".

References

García-Lafuente, J., Sánchez-Román, A., Díaz del Río, G., Sannino, G., and J. C. Sánchez-Garrido, 2007. Recent observations of seasonal variability of the Mediterranean outflow in the Strait of Gibraltar. J. Geophys. Res., 112, C10005, doi:10.1029/2006JC003992.

Kinder, T.H., Parrilla, G., 1987. Yes, some of the Mediterranean outflow does come from great depths. Journal of Geophysical Research, 92, C3, 2901-2906.

MEDAR Group: MEDATLAS/2002 database. Mediterranean and Black Sea database of temperature salinity and bio-chemical parameters. Climatological Atlas. IFREMER Edition (4 CDroms) , 2002.

Millot, C., 1985. Some features of the Algerian Current. J. Geophys. Res., 90, C4, 7169-7176.

Millot, C., 1987. Circulation in the Western Mediterranean. Oceanol. Acta, 10, 2, 143-149.

Millot C., 1999. Circulation in the Western Mediterranean Sea. J. Mar. Systems, 20, 1-4, 423-442.

Millot, C. , 2007. Interannual salinification of the Mediterranean inflow. Geophysical Research Letters, 34, L21069, doi:10.1029/2007/GL031179.

Millot, C. , 2008. Short-term variability of the Mediterranean in- and out-flows. Geophysical Research Letters, 35, L15603, doi:10.1029/2008/GL033762

Millot, C. , 2009. Another description of the Mediterranean Sea outflow. Progress in Oceanography, vol. 82, iss. 2, 101-124,doi:10.1016/j.pocean.2009.04.016

Millot, C., submitted. The LIW characteristics: and astounding general misunderstanding! Submitted to Scientia Marina. Available at: http://www.ifremer.fr/lobtln/.

Millot, C. and Briand, F., 2002. Executive summary. In *"Tracking long term hydrological change in the Mediterranean Sea"*. (ed Briand, F.) 7-14 (CIESM Workshop Series n°16), http://www.ciesm.org/online/monographs/Monaco02.html

Millot, C., Candela, J., Fuda, J.-L., and Tber, Y. , 2006. Large warming and salinification of the Mediterranean outflow due to changes in its composition. Deep-Sea Res., 53/4, 656-666, doi:10.1016/j.dsr.2005.12.017.

Millot, C., and Garcia-Lafuente, J., 2011. The seasonal and fortnightly variability of the Mediterranean outflow. Ocean Sciences, 7, 1-8, doi:10.5194/os-7-1-2011.

Schroeder K., J. Garcìa-Lafuente, S.A. Josey, V. Artale, B. Buongiorno Nardelli, A. Carrillo, M. Gačić, G.P. Gasparini, M. Herrmann, P. Lionello, W. Ludwig, C. Millot, E. Özsoy, G. Pisacane, J.C. Sánchez-Garrido, G. Sannino, R. Santoleri, S. Somot, M. Struglia, E. Stanev, I. Taupier-Letage, M.N. Tsimplis, M. Vargas-Yáñez, V. Zervakis, G. Zodiatis, 2011. *Chapter 4: Circulation of the Mediterranean Sea and its variability*. In: Mediterranean Climate: from past to future. Ed. P. Lionello. In press.

Stommel , H., H. Bryden and P. Mangelsdorf. Does some of the Mediterranean outflow come from great depth? Pure Appl. Geophys., 105, 879-889, 1973.

Legends captions

Figure 1. The study area with the schematized circulation of the AWs (SAW, NACW), the intermediate MWs (WIW, LIW, TDWi) and the deep MWs (TDWd, WMDW). While the two former sets of waters circulate significantly (thick arrows), the latter circulate only sluggishly (thin arrows) and deep MWs are mainly uplifted in the Alboran subbasin up to the eastern entrance of the strait. Colours associated with each of the waters are those used for all figures in chapter 2, but they have nothing to do with the colours associated with the CTD time series (triangles in the yellow rectangle enlarged in Fig.2) used for all figures in chapter 3. The GIBEX transects are schematized in blue.

Figure 2. The autonomous CTDs are operated on short (~10 m height) subsurface moorings that are serviced every 1-2 years at C, M and E while they were deployed only once at ES and EN. Accurate positions are systematically obtained by acoustic triangulation while depth is more accurately specified from a fine-resolution bathymetric data set (Antonio Sanchez-Roman, pers. com.). When redeploying a CTD, its nominal position is reached with a few 10s m accuracy at M, within no more than 100 m at both C and E. Nominal positions and depths are: C (35°55.2' N-5°45.0' W, 270 m), M (35°52.8' N-5°43.5' W, 80 m), E (35°51.7' N-5°58.5' W, 360 m), ES (35º50.56' N-5º58.40' W, 320 m), EN (35°52.65' N-5º58.46' W, 320 m). Note in particular that the Camarinal transect (at 5.75'W=5°45'W) used

in Fig.4 and Fig.31 does not clearly evidence the two sills that would be more clearly evidenced by a north-west to south-east transect.

Figure 3. a) Definition of the AWs using profiles 3 (data as cyan and green dots) and 4 (data as cyan-blue dots) from the GIB2 transect at 6°05'W together with a profile from the LYNCH campaign along the same transect (grey dots). Profiles (links between the data) are in black and isopycnals are in kg.m^{-3}; see text for details. b) Definition of the MWs (data as coloured dots without any link between them) using profile 6 from the GIB2 transect at 4°30'W together with schematized mixing lines between any of the MWs and an unspecified AW. The mixing lines for TDW and the dashed black lines schematize the relationships evidenced between the C and E time series by MGL11; see text for explanations about the -20°, -40° and +75° slopes, and other details as well.

Figure 4. Bathymetric data along the GIB transects and across the southern sill of Camarinal (5°45'W) and the sills of Espartel (5°58,5'W) inferred not from navigation charts with a 5-nm interval (as in M09) but from the ETOPO-1nm data base for transects at 4°30'W, 5°00'W and 5°15'W, and from small scale bathymetric surveys for the other transects (Antonio Sanchez-Roman, pers. com.). The AWs-MWs interface (σ=28.0 kg.m^{-3} for all transects except the 6°15'W one for which we choose σ=27.8 kg.m^{-3} in violet) is represented in red for both GIB1 (full) and GIB2 (dashed). The blue isopycnal is σ=29.08 kg.m^{-3} for all transects up to 5°40'W, while it is in cyan for σ=28.75 kg.m^{-3} and σ=28.5 kg.m^{-3} at 5°50'W and 6°05'W-6°15'W, respectively.

Figure 5. Distribution of S during GIB1 at some nominal depths (averaged in the range ±5 m) between 5 and 100 m. Coloration, size and orientation of the arrows are commented in the text.

Figure 6. θ-S diagram focusing on the AWs, θ-S diagram focusing on the MWs and σ section at 4°30'W during GIB1. Plotted on this section are some isopycnals (in kg.m^{-3}): 26.9 (thin; limit between SAW in cyan and NACW in green; out of range here), 28.0 (thick; definition of the AWs-MWs interface), 28.75 (dashed; definition of the AWs-MWs interface in M09), 29.0 (thin; lower limit of WIW in orange), 29.075 (thin; lower limit of LIW in red), 29.08 (thick; definition of the light/intermediate – dense/deep MWs used by M09), as well as the 12.85 °C isotherm (limit between TDW in magenta and WMDW in blue) and the AWs-MWs interface inferred from the maximum S and σ vertical gradients (thick yellow line). See text for other definitions and notes.

Figure 7. As in Figure 6 for 5°00'W.

Figure 8. As in Figure 6 for 5°15'W. Note the 26.9 kg.m^{-3} isopycnal.

Figure 9. As in Figure 6 for 5°30'W.

Figure 10. As in Figure 6 for 5°40'W. The plotted mixing line is the best linear fit for all data from p1 and p2 between S=37.5 (~100 m) and S~38.45; it will be plotted at 5°50'W as a dashed line ranging from the less mixed values at 5°40'W to the less mixed values at 5°50'W (and so on for the other transects).

Figure 11. As in Figure 6 for 5°50'W, except for the isopycnals plotted in the σ section that are (in kg.m^{-3}) below 28.0 (the AWs-MWs interface): 28.5 (thin), 28.75 (thick) and 28.97 (dashed). The mixing line computed there for TDW considers all data from both p1 and p2 between S=37.8 (210-220 m, i.e. nearly the AWs-MWs interface there) and 38.39. The mixing line computed from p3 and associated with LIW considers data between S=37.8 (here at 180 m, i.e. near the AWs-MWs interface) and S=38.386. The mixing line computed from

p6-p7 and associated with WIW considers data between S=37.8 (190-200 m, i.e. not far from the AWs-MWs interface) and S=38.275.

Figure 12. As in Figure 6 for 6°05'W except for the isopycnals plotted in the σ section that are (in kg.m^{-3}): 26.9 (thick), 27.0 (dashed), 27.5 (thin), 28.0 (thick; the AWs-MWs interface), 28.5 (thick) and 28.75 (thin). Mixing lines are associated with TDW (computed from p1 data between S=37.5 (260 m) and S=38.224), LIW (computed from the p2-p3 data between S=37.15 (230 m, exactly at the AWs-MWs interface) and S=38.289) and WIW (computed from p4 data between S=37.2 (265 m, at the AWs-MWs interface) and 38.058).

Figure 13. As in Figure 6 for 6°15'W except for the isopycnals plotted in the σ section that are (in kg.m^{-3}): 26.9 (thick), 27.0 (dashed), 27.5 (thin), 27.8 (thick; the AWs-MWs interface), 28.0 (dashed), 28.5 (thick) and 28.75 (thin).

Figure 14. Distribution of S during GIB2 at some nominal depths (averaged in the range ±5 m) between 5 and 100 m. Coloration, size and orientation of the arrows are specified in the text.

Figure 15. As in Fig.6 (4°30'W) for GIB2. Note the stratification in the AWs-MWs layer schematized by σ=26.9 kg.m^{-3}.

Figure 16. As in Figure 6 for 5°00'W and GIB2.

Figure 17. As in Figure 6 for 5°15'W and GIB2.

Figure 18. As in Figure 6 for 5°30'W and GIB2.

Figure 19. As in Figure 6 for 5°40'W and GIB2. Mixing lines are associated with WIW (computed from data at p6 between S=37.4 (nearly the AWs-MWs interface) and S=38.319), TDW (computed from data at p2 in the S range 38.0-38.4) and WMDW (computed from data at p1 in the S range 37.6-38.431).

Figure 20. As in Figure 11 for GIB2 and the densest isopycnal in the σ section being 29.01 kg.m^{-3} (dashed). Mixing lines are associated with WIW (computed from data at p6 in the S range 37.65-38.172), LIW (computed from data at p5, one in the S-ranges 38.304-38.352, and one in the S range 38.228-38.268), WMDW (computed from the data at p1-p2 in the S range 37.7-38.398).

Figure21. As in Figure 12 for GIB2. Mixing lines are associated with LIW (computed from data at p4 in the S range 37.807-38.047) and WMDW (computed from data at p3 in the S range 38.105-38.285).

Figure 22. As in Figure 13 for GIB2.

Figure 23. Density (σ in kg.m^{-3}) time series at C (red), E (blue) and ES (violet) during a 128-day period in October 2007-March 2008; see positions in Fig.2. The fortnightly time scale is emphasized.

Figure 24. Potential temperature (θ; descending axis), salinity (S), density (σ) and slope of the temporal mixing line (A) inferred from filtered (25-h median) 1-h time series at E (blue) and ES (violet).

Figure 25. θ-S diagrams showing the E+ES and E+EN time series during the 128-day and 64-day periods, respectively, with black arrows indicating mixing lines slopes of -40° and -20° associated (see MGL11) with some kind of SAW and some kind of NACW, respectively. The acronym MWs indicates "the less mixed MWs" since all MWs are partially mixed with the AWs at the longitude of the sills of Espartel. a) original time series at E (blue) and ES (violet); b1 and b2) original time series at E (blue) and EN (cyan) showing the same time

series with one or the other in forward position; c) the original E (blue) and EN (cyan) time series shown in b1-b2 together with the intersections (brown) of the E and EN mixing lines; d) same as in c) for filtered (median / 25 h) data; e) same as in c) in different ranges and additional information detailed in the text.

Figure 26. S, θ and the associated mixing lines slopes (MLS=Δθ/ΔS; shown instead of parameter A since used in the computations) at E (blue) and C (red) during the 128-day period. Assuming that the MWs encountered at E are those encountered at C and starting from a point θ(E)-S(E), the associated mixing line with the slope MLS(E) defines, at S(C), a θinferred(C) that can be compared with the measured θ(C). Comparing the absolute differences δθ between θ(E) and θ(C) in light grey with those between θinferred(C) and θ(C) in dark grey allows appreciating the validity of the hypothesis. Similar results (not shown) are obtained for the 2004-2008 period analyzed by MGL11. Additional X-axes (S=38.4, θ=13.1°C, δθ=0 °C, MLS=-40 °C) are the same for the other similar figures (27 and 29).

Figure 27. Same as in Fig.26 for ES (violet) and C (red).

Figure 28. Potential temperature (θ; descending axis), salinity (S), density (σ) and slope of the temporal mixing line (A) inferred from filtered (25-h median) 1-h time series at E (blue) and EN (cyan) during the 64-day period.

Figure 29. Same as in Fig.26 for the 64-day period (reduced to 21 days since C was serviced meanwhile): a) EN (cyan) and C (red), b) E (blue) and C (red).

Figure 30. Schematization of the AWs-MWs mixing processes: a) from the Atlantic Ocean, across the Strait of Gibraltar (the minimum depths there schematize the sills of Espartel and Camarinal), to the Mediterranean Sea (the western part of the Alboran subbasin). The dashed line represents the interface between the AWs (cyan, NACW and SAW are not differentiated) and the MWs (represented by TDW in magenta). Unmixed waters are schematized, at some specific longitudes, with thick lines plotted at a given constant distance from the longitude they are associated with. This distance being +0.1° for the MWs and -0.1° for the AWs, the lines could represent the salinity. In the layer where AWs and MWs are mixed, mixing lines are represented by both colours and they necessarily define, at all specific longitudes, the AWs-MWs interface we have chosen to be as simple as possible, which can give, in addition to the features we wanted to schematize, some other unrealistic ones. b) for the AWs and both WIW and LIW. c) for the AWs and WMDW (or TDWd).

Figure 31. Schematization of the structure of the Atlantic inflow, with its two components, and of the Mediterranean outflow, with three intermediate/light and one deep/dense MWs: SAW (cyan), NACW (green), WIW (orange), LIW (red), TDW (pink) and WMDW (blue). Note that only the intermediate part of TDW (namely TDWi) is represented while its deep part (namely TDWd) is often encountered instead of WMDW.

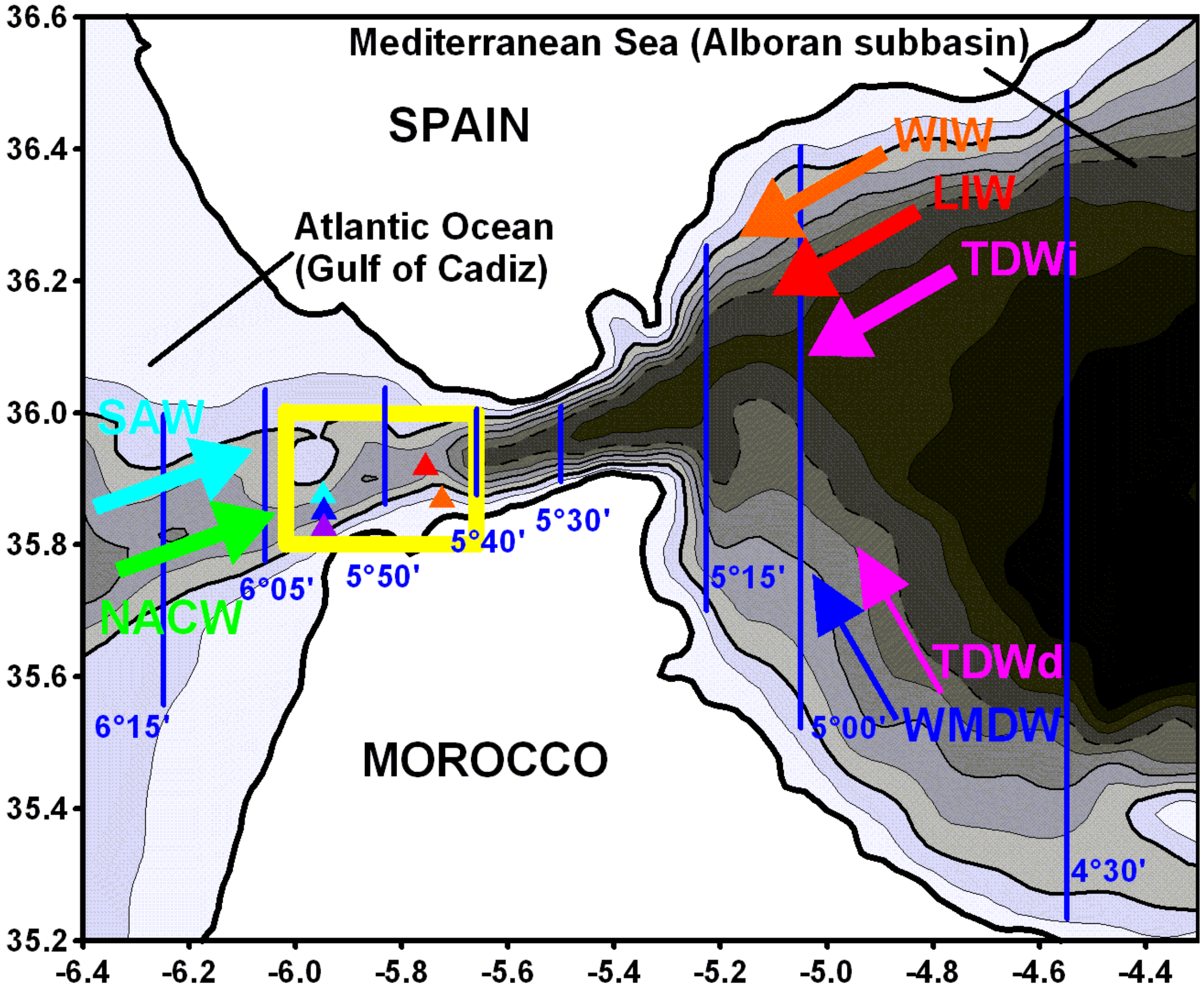
Mediterranean Sea (Alboran subbasin)
SPAIN
Atlantic Ocean
(Gulf of Cadiz)
MOROCCO
SAW
NACW
WIW
LIW
TDWi
TDWd
WMDW
6°15'
6°05'
5°50'
5°40'
5°30'
5°15'
5°00'
4°30'
36.6
36.4
36.2
36.0
35.8
35.6
35.4
35.2
-6.4
-6.2
-6.0
-5.8
-5.6
-5.4
-5.2
-5.0
-4.8
-4.6
-4.4

Figure 1

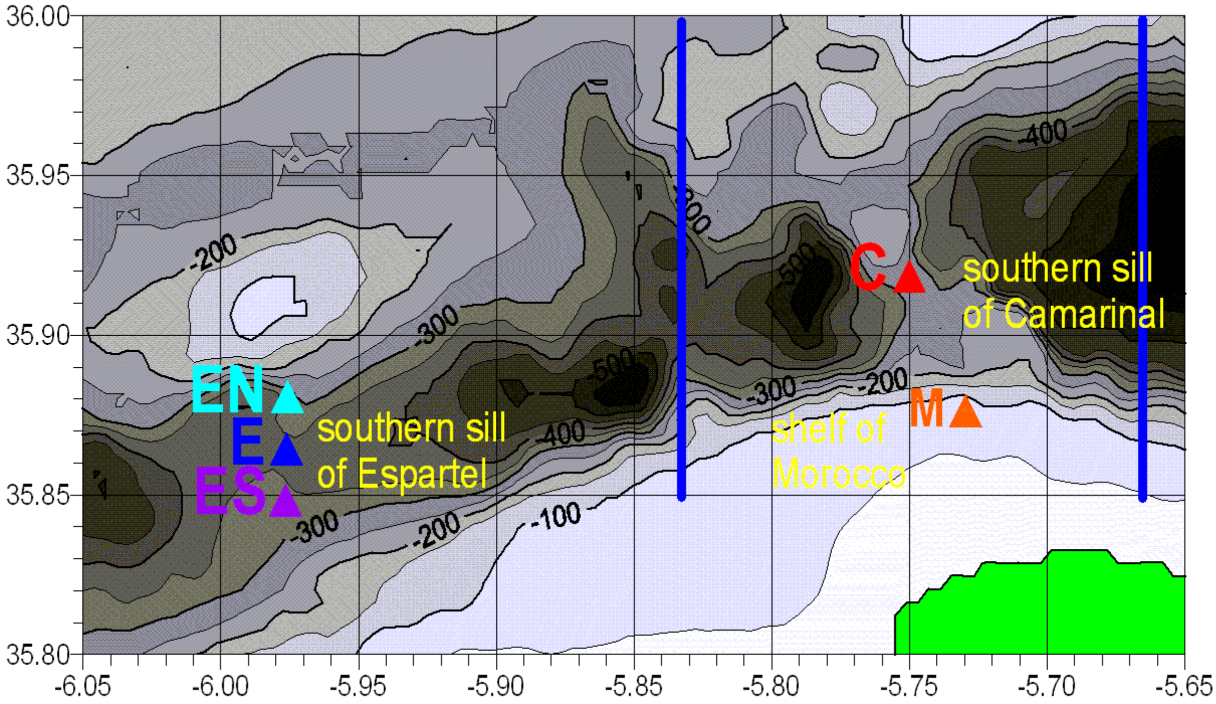

36.00
35.95
35.90
35.85
35.80
-6.05
-6.00
-5.95
-5.90
-5.85
-5.80
-5.75
-5.70
-5.65
EN
E
ES
southern sill
of Espartel
C
southern sill
of Camarinal
M
shelf of
Morocco
-100
-200
-300
-400
-500

Figure 2

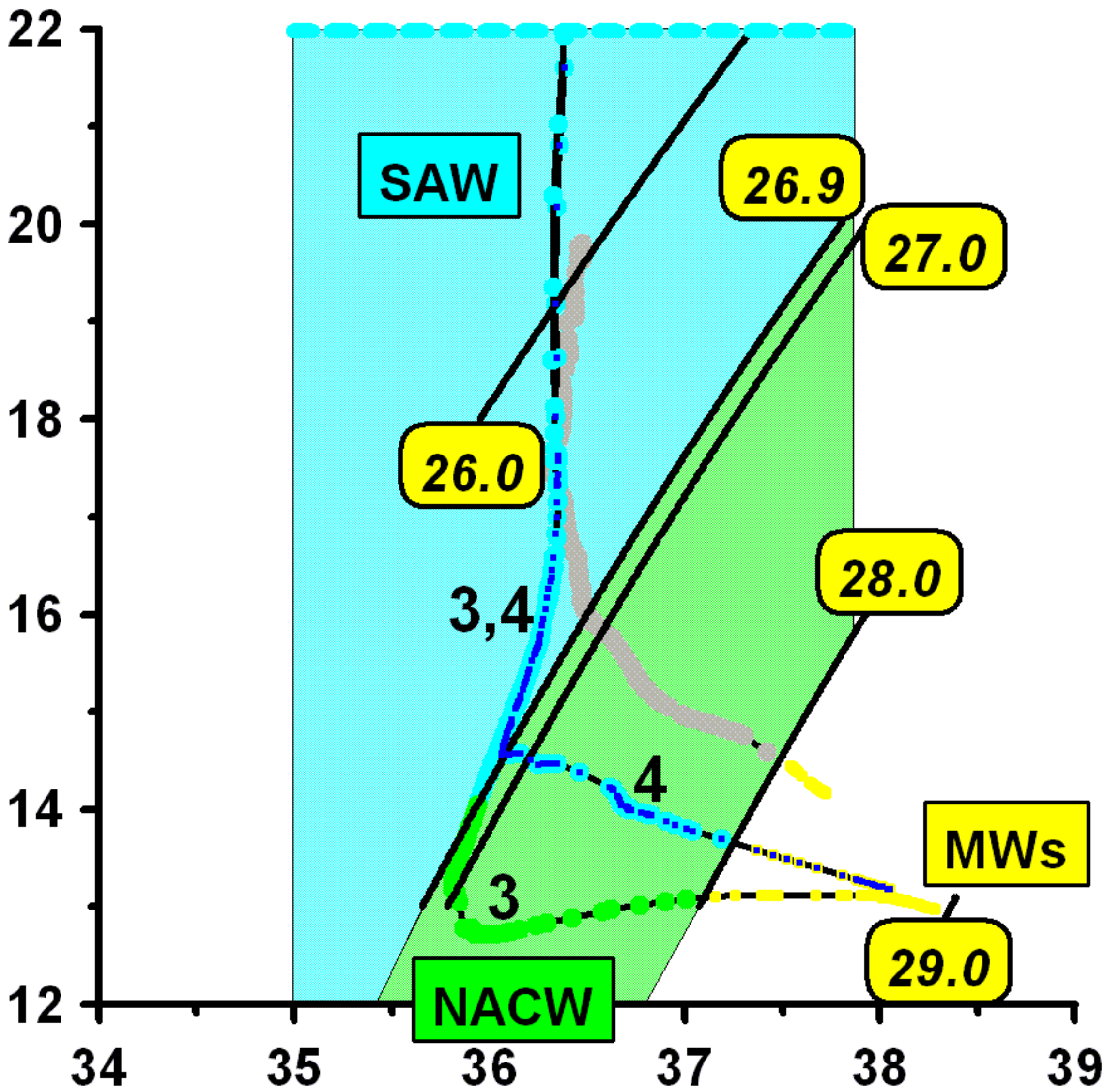
22
20
18
16
14
12
34
35
36
37
38
39
SAW
26.9
27.0
26.0
28.0
3,4
4
3
MWs
29.0
NACW

Figure 3a

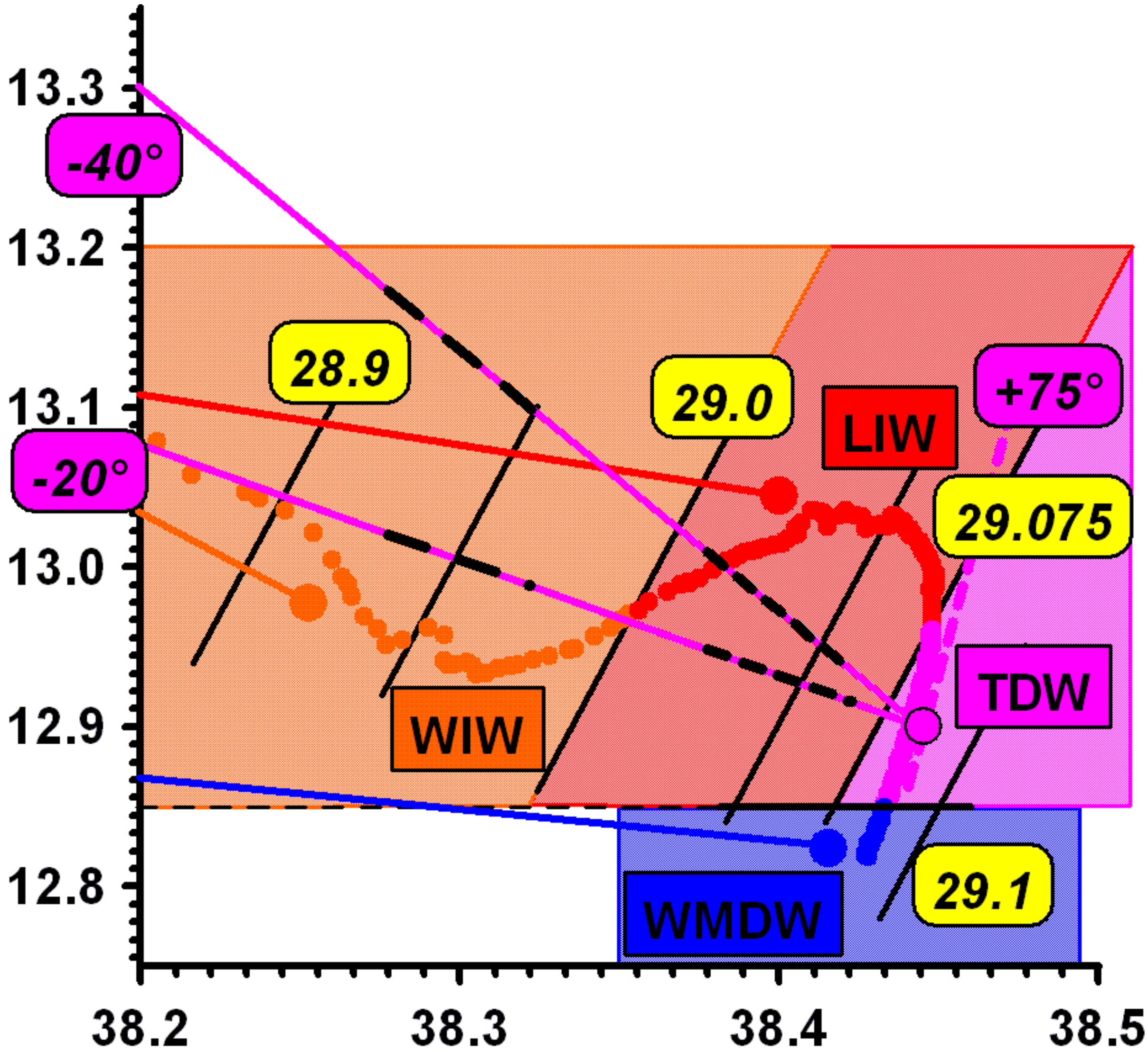
13.3
13.2
13.1
13.0
12.9
12.8
38.2
38.3
38.4
38.5
-40°
-20°
+75°
28.9
29.0
29.075
29.1
LIW
WIW
TDW
WMDW

Figure 3b

1

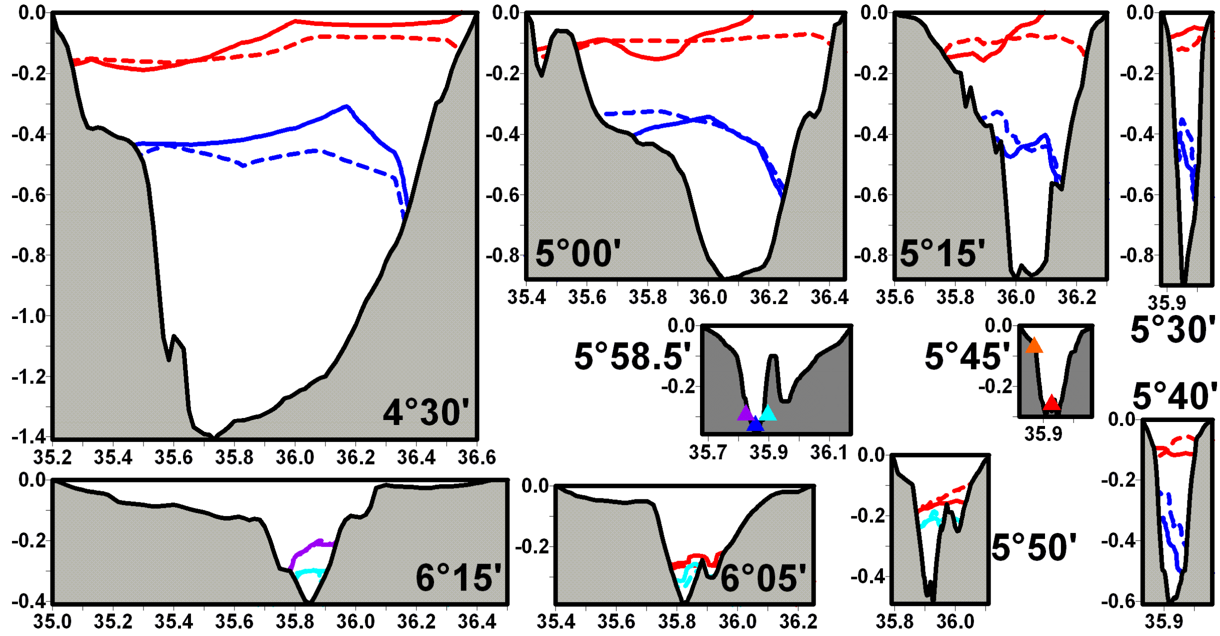

2 Figure 4

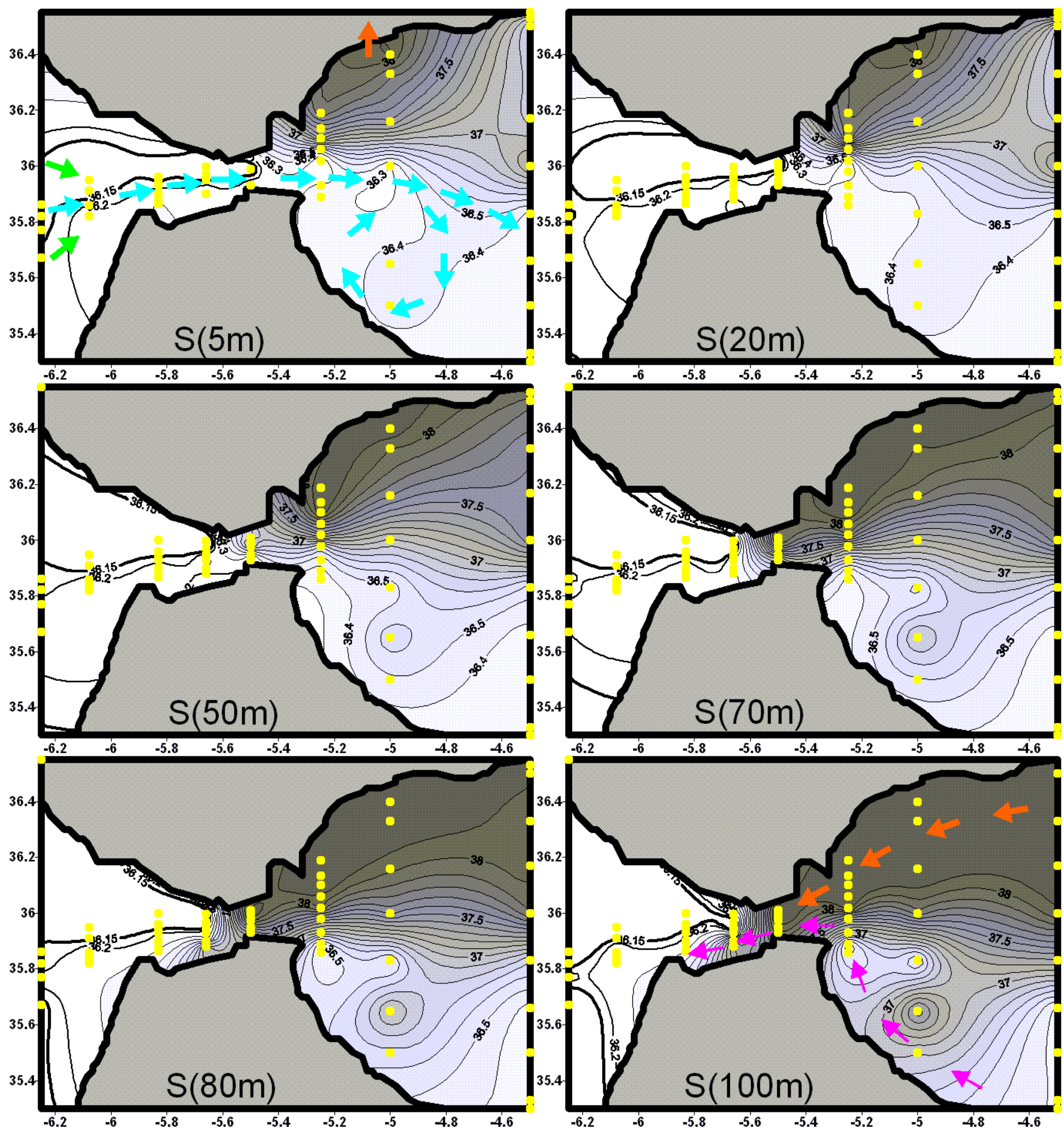

1

2 Figure 5

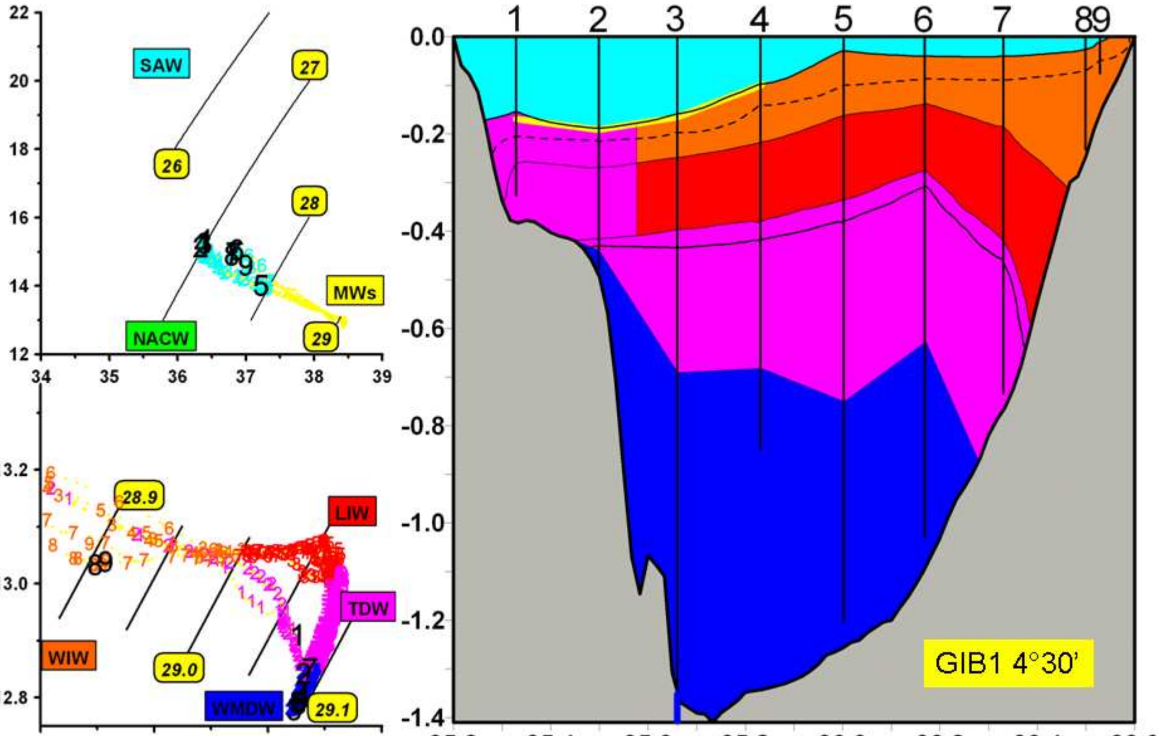

Figure 6

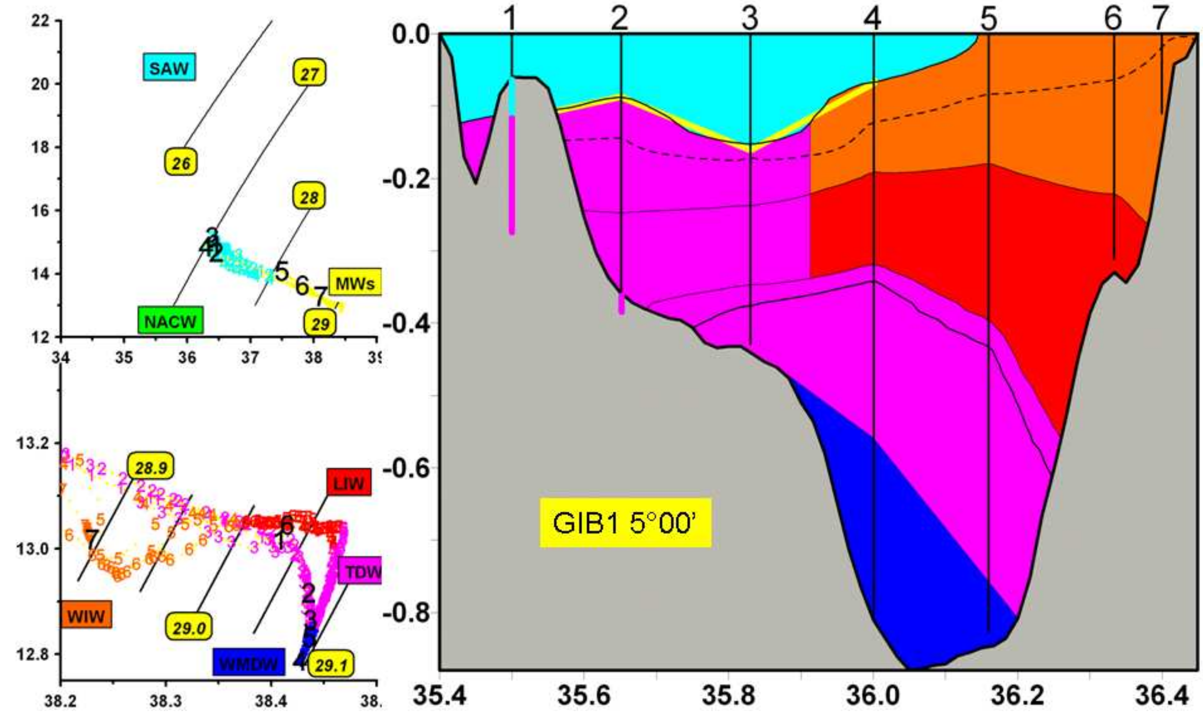

Figure 7

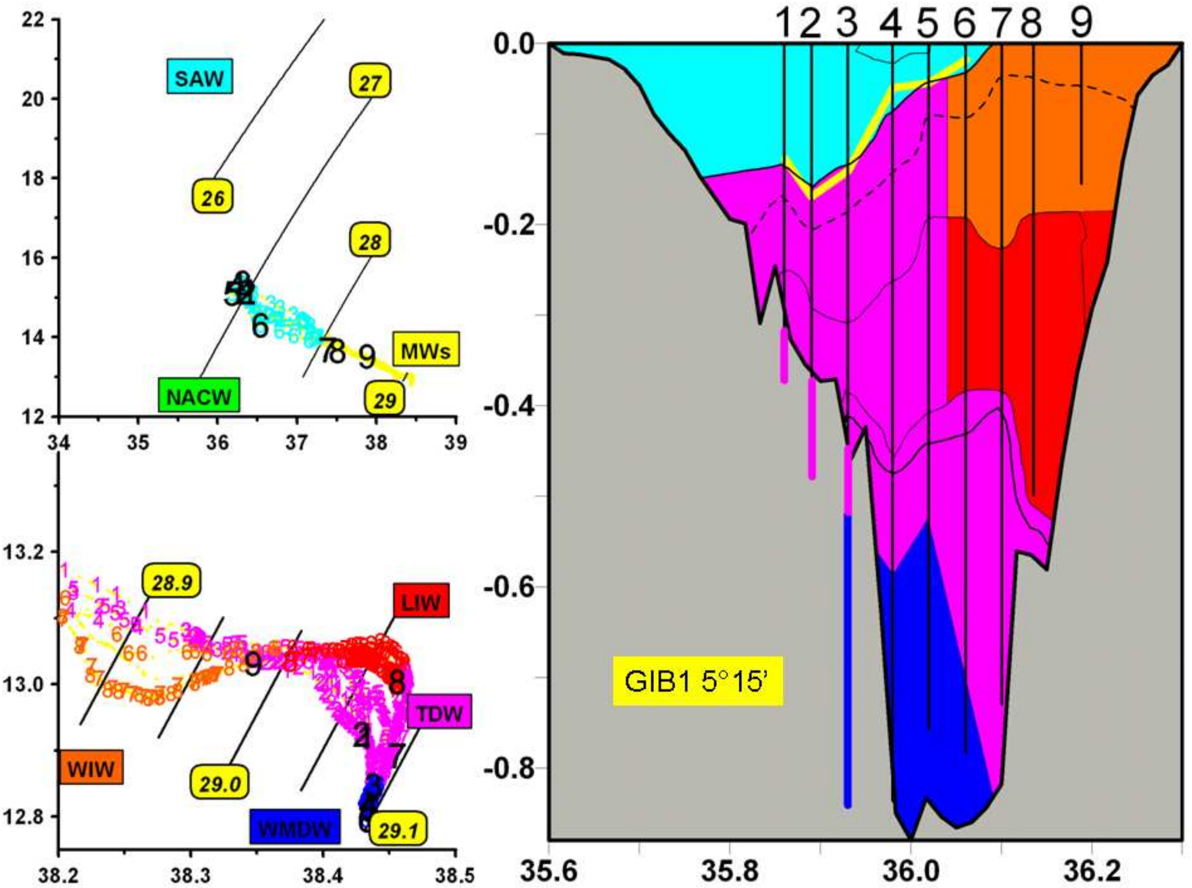
SAW
NACW
MWs
26
27
28
29
LIW
TDW
WIW
WMDW
28.9
29.0
29.1
GIB1 5° 15'
1 2 3 4 5 6 7 8 9

Figure 8

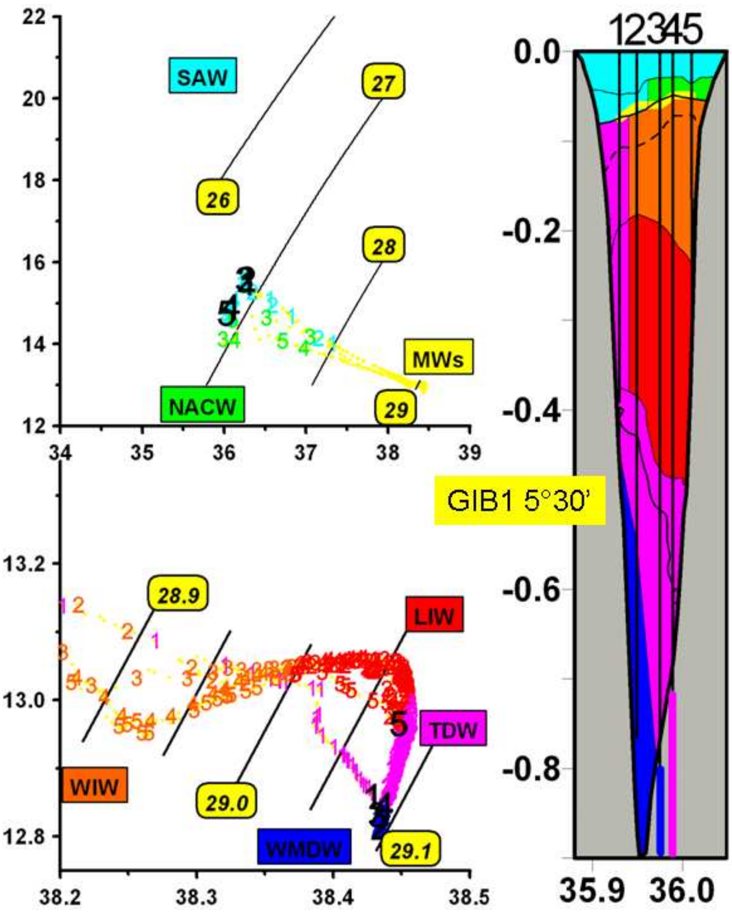

SAW
NACW
MWs
26
27
28
29
LIW
TDW
WIW
WMDW
28.9
29.0
29.1
GIB1 5°30'
12345
0.0
-0.2
-0.4
-0.6
-0.8
35.9
36.0

1
2 Figure 9

1

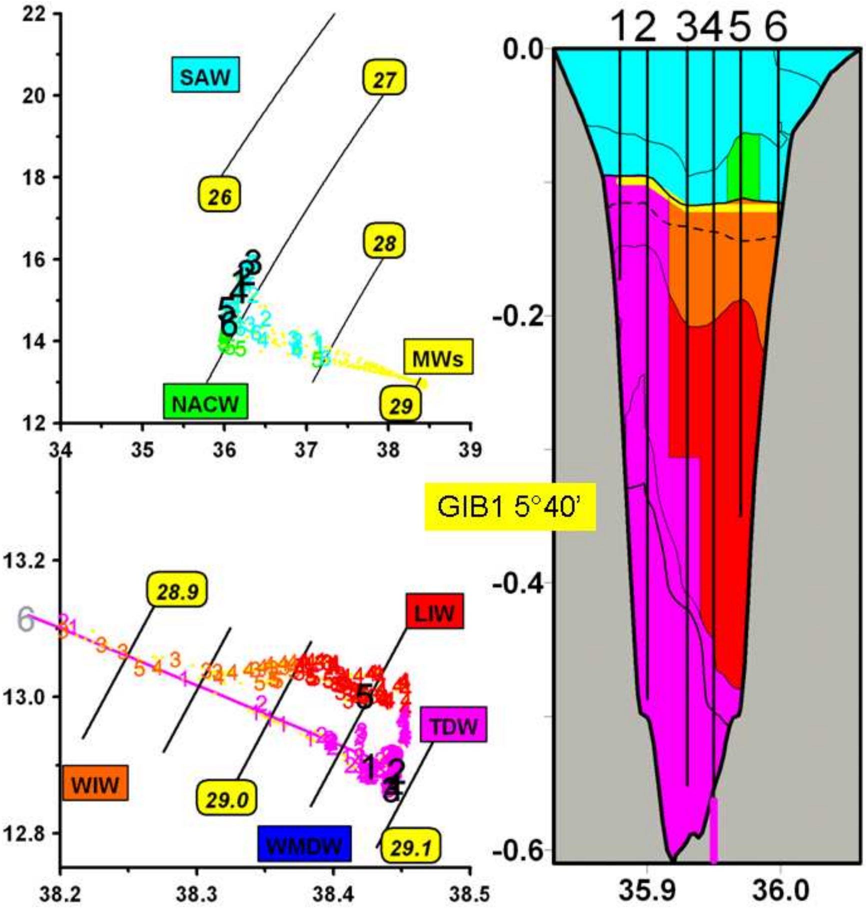
SAW
26
27
28
NACW
MWs
29
28.9
LIW
TDW
WIW
29.0
WMDW
29.1
GIB1 5°40'
1 2 3 4 5 6
0.0
-0.2
-0.4
-0.6
35.9
36.0

2 Figure 10

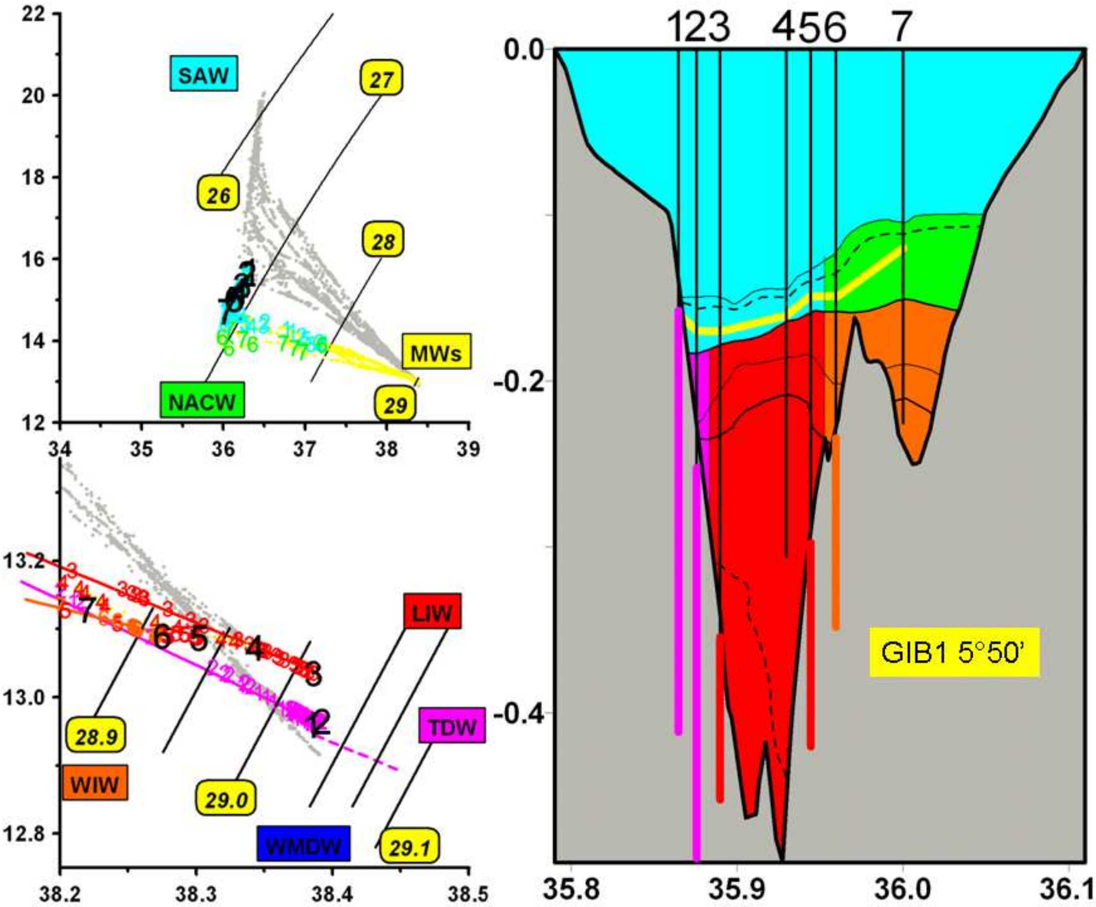
SAW
NACW
MWs
26
27
28
29
LIW
TDW
WIW
WMDW
28.9
29.0
29.1
1 2 3 4 5 6 7
0.0
-0.2
-0.4
GIB1 5°50'
35.8
35.9
36.0
36.1
22
20
18
16
14
12
34
35
36
37
38
39
13.2
13.0
12.8
38.2
38.3
38.4
38.5

Figure 11

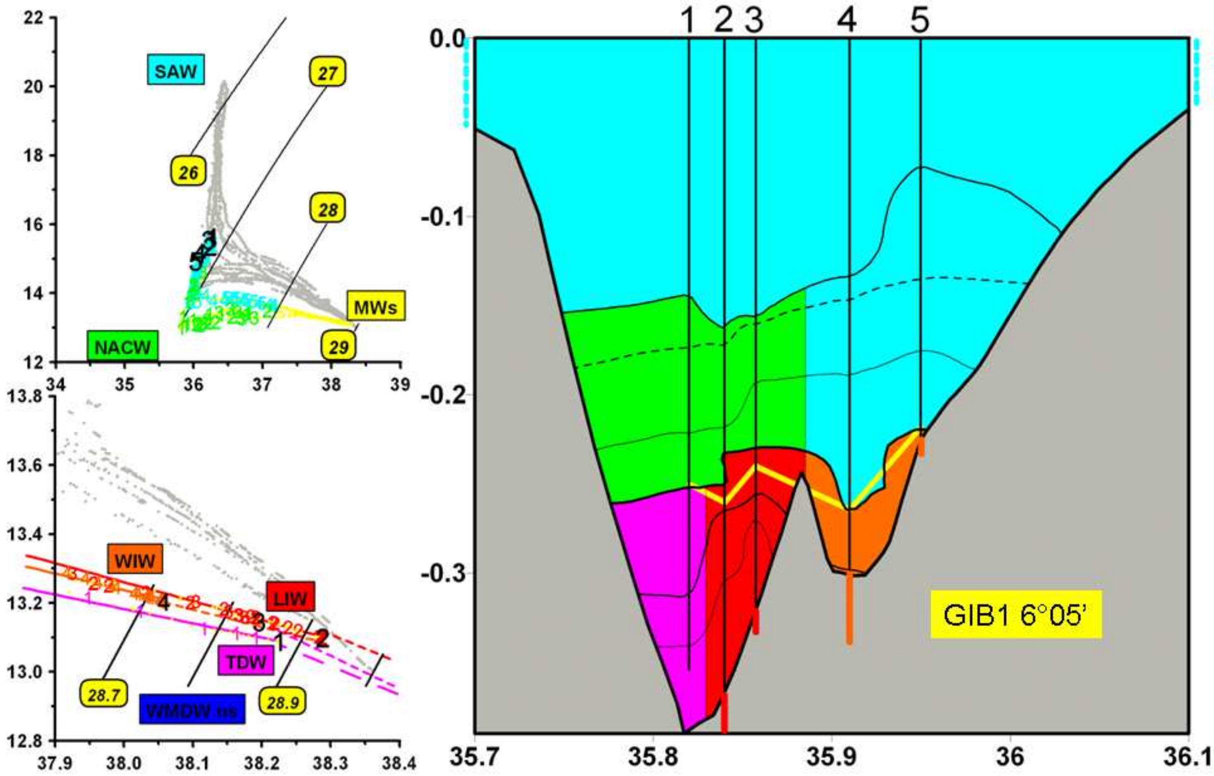

Figure 12

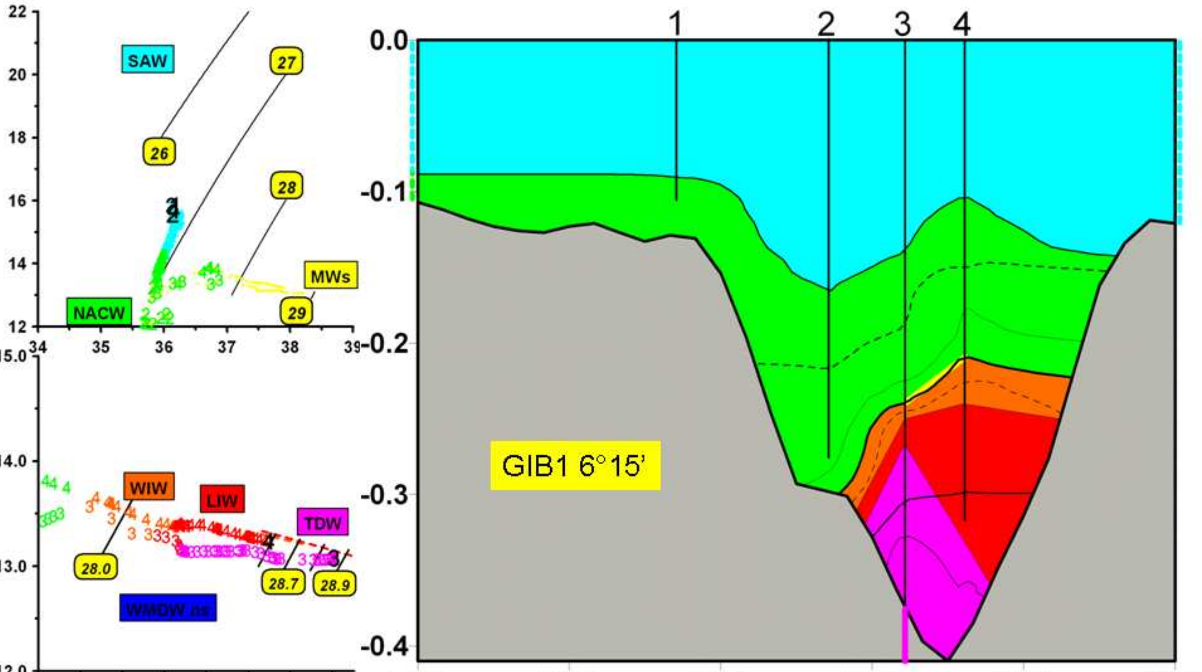

SAW
26
27
28
MWs
NACW
29
WIW
LIW
TDW
28.0
28.7
28.9
GIB1 6° 15'
1
2
3
4
0.0
-0.1
-0.2
-0.3
-0.4
35.5
35.6
35.7
35.8
35.9
36.0

Figurre 13

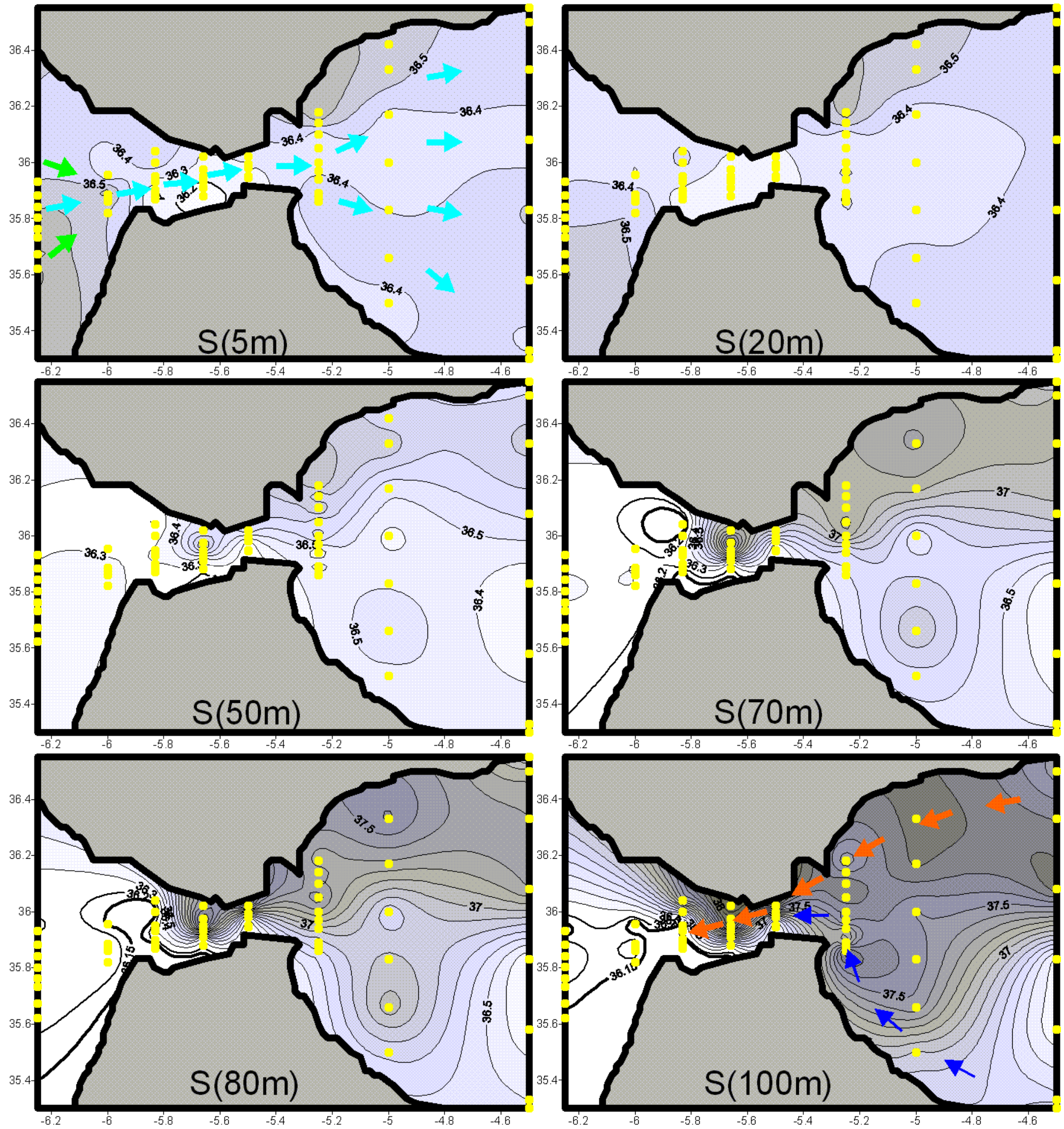

Figure 14

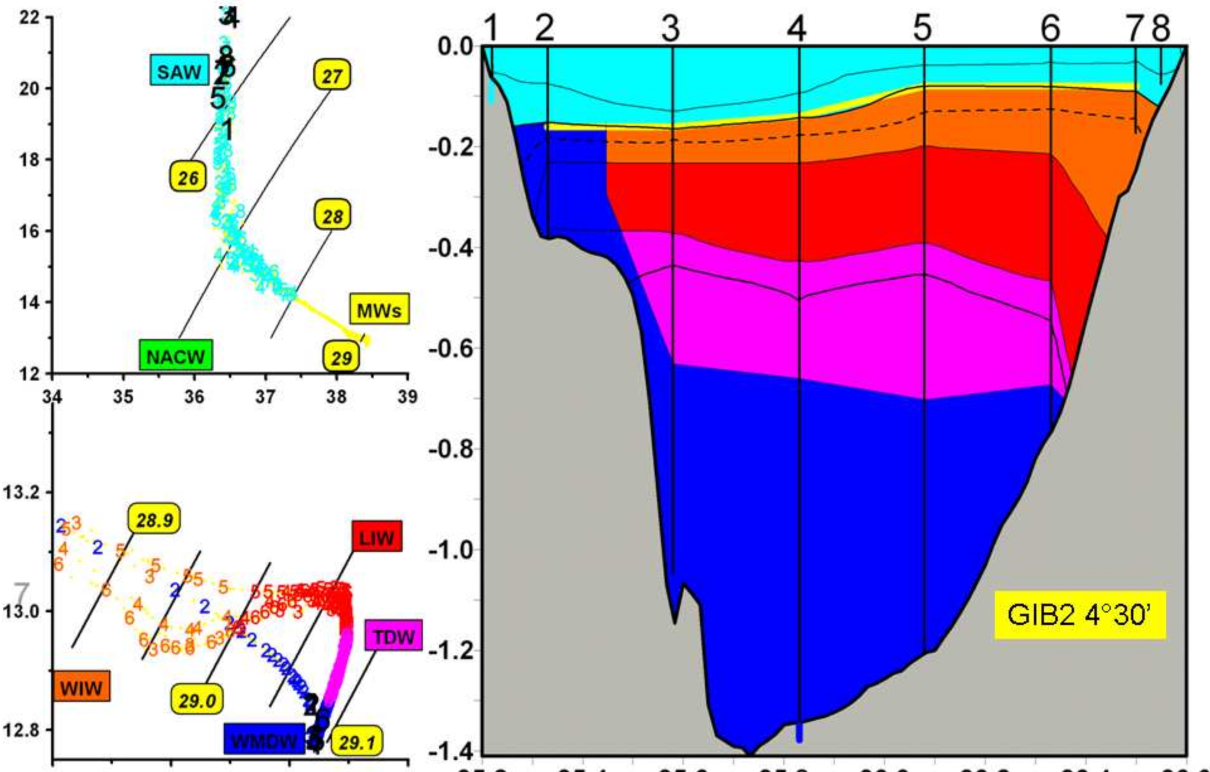

Figure 15

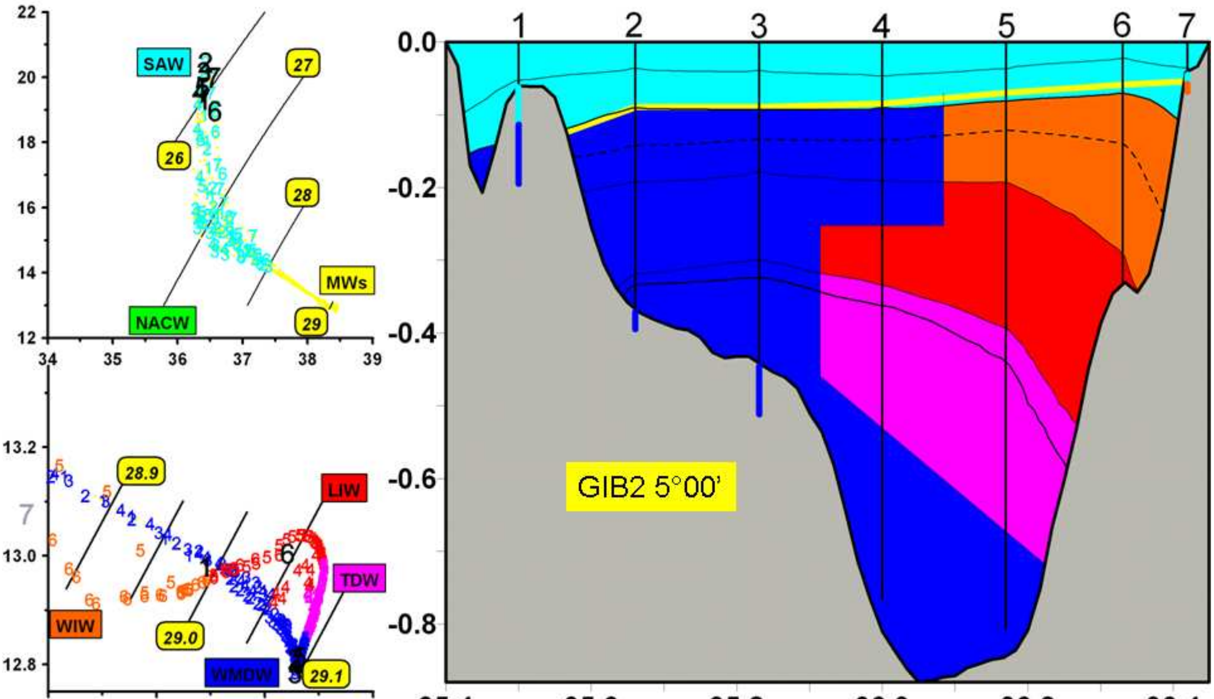

SAW
NACW
MWs
26
27
28
29
22
20
18
16
14
12
34
35
36
37
38
39
13.2
13.0
12.8
38.2
38.3
38.4
38.5
28.9
29.0
29.1
LIW
TDW
WIW
WMDW
1
2
3
4
5
6
7
0.0
-0.2
-0.4
-0.6
-0.8
35.4
35.6
35.8
36.0
36.2
36.4
GIB2 5°00'

Figure 16

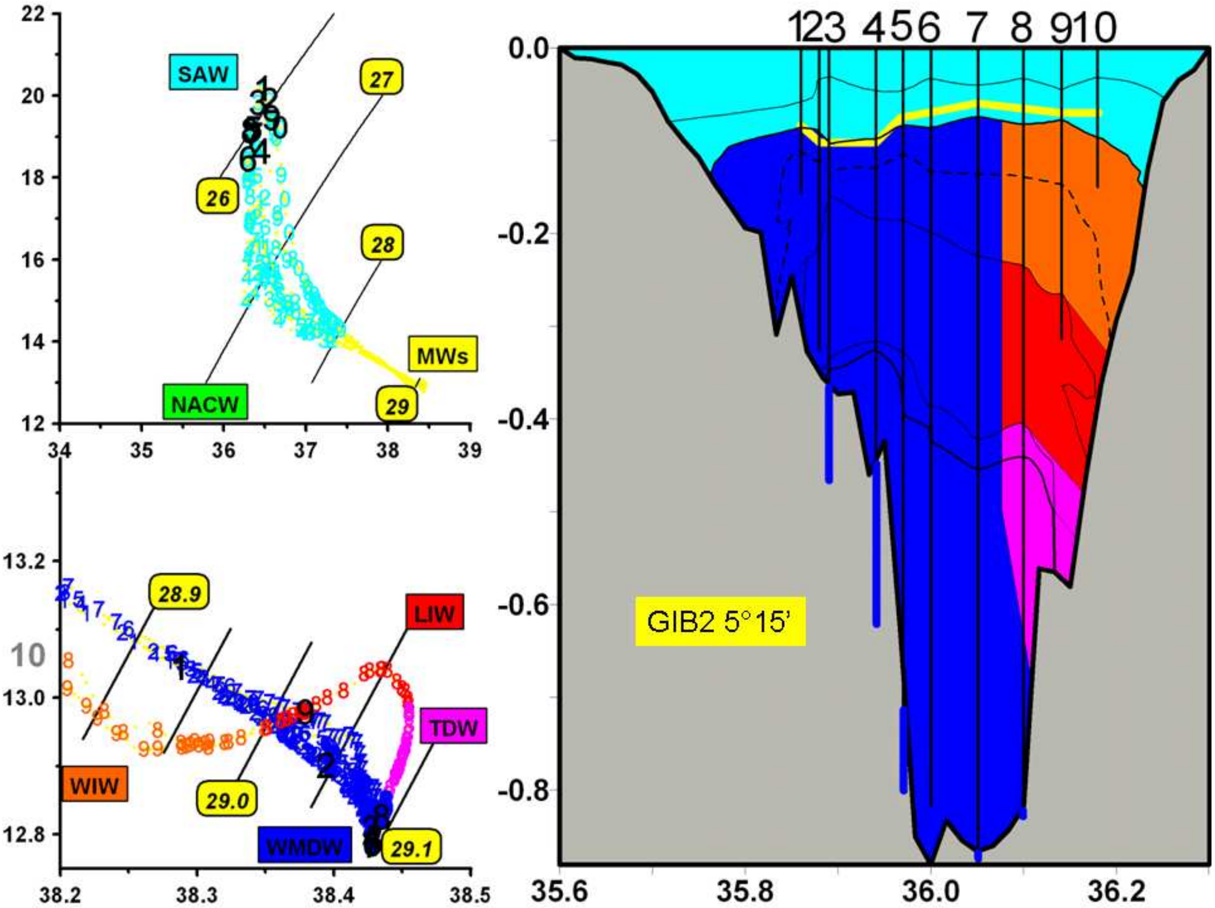

SAW
26
27
28
MWs
29
NACW
22
20
18
16
14
12
34
35
36
37
38
39
13.2
13.0
12.8
10
28.9
29.0
29.1
LIW
TDW
WIW
WMDW
38.2
38.3
38.4
38.5
1 2 3 4 5 6 7 8 9 10
0.0
-0.2
-0.4
-0.6
-0.8
GIB2 5° 15'
35.6
35.8
36.0
36.2

Figure 17

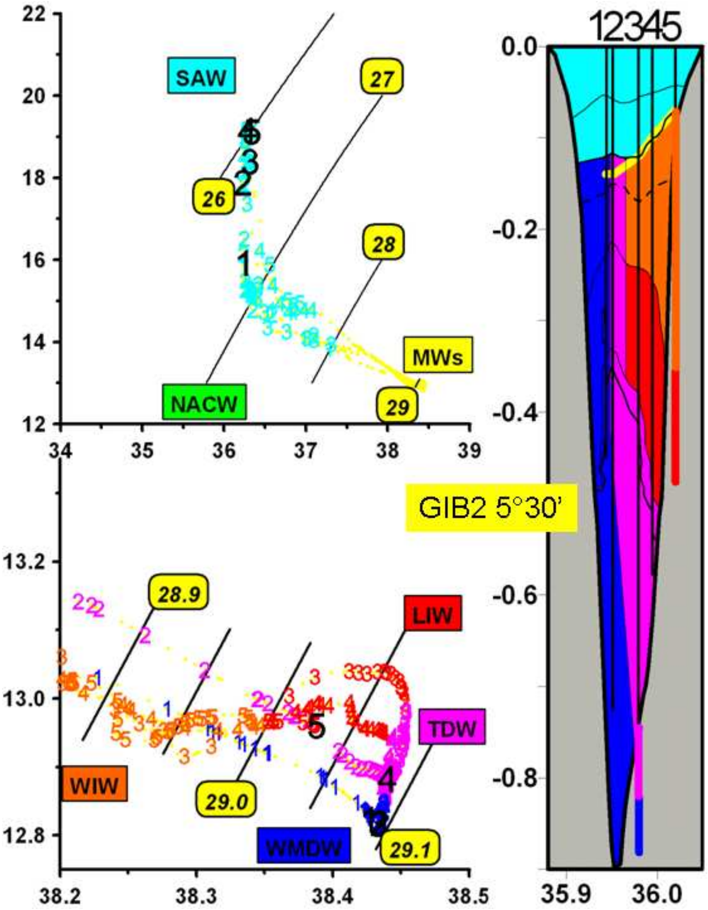
SAW
NACW
MWs
26
27
28
29
GIB2 5°30'
12345
28.9
29.0
29.1
LIW
TDW
WIW
WMDW
22
20
18
16
14
12
34
35
36
37
38
39
13.2
13.0
12.8
38.2
38.3
38.4
38.5
0.0
-0.2
-0.4
-0.6
-0.8
35.9
36.0

Figure 18

1
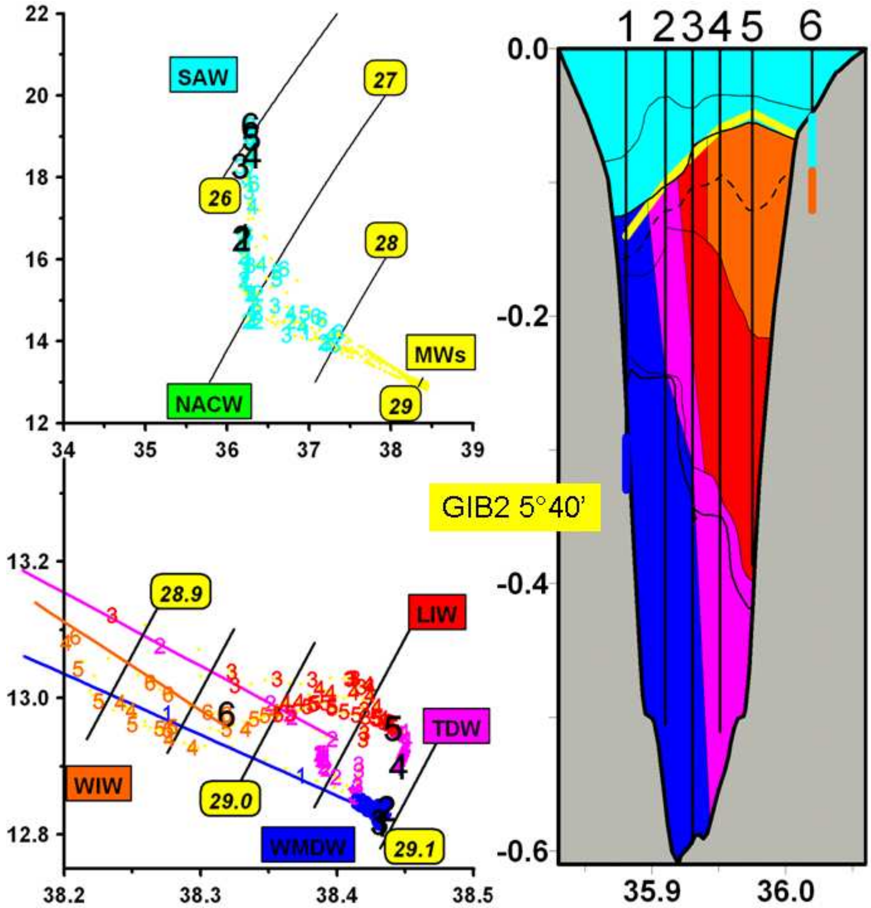
SAW
NACW
MWs
26
27
28
29
22
20
18
16
14
12
34
35
36
37
38
39
13.2
13.0
12.8
38.2
38.3
38.4
38.5
28.9
29.0
29.1
LIW
TDW
WIW
WMDW
1 2 3 4 5 6
0.0
-0.2
-0.4
-0.6
35.9
36.0
GIB2 5°40'

2 Figure 19

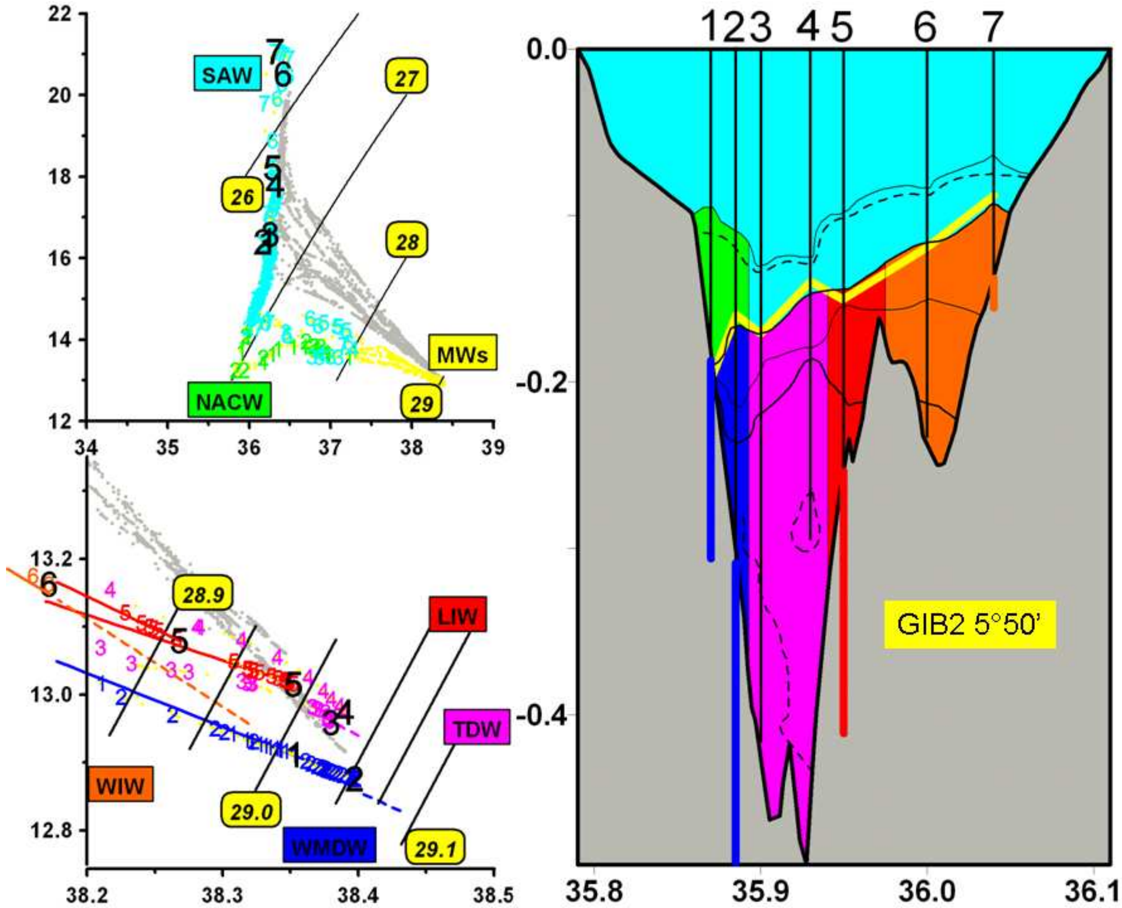
SAW
NACW
MWs
26
27
28
29
22
20
18
16
14
12
34
35
36
37
38
39
WIW
LIW
TDW
WMDW
28.9
29.0
29.1
13.2
13.0
12.8
38.2
38.3
38.4
38.5
1 2 3 4 5 6 7
0.0
-0.2
-0.4
GIB2 5°50'
35.8
35.9
36.0
36.1

Figure 20

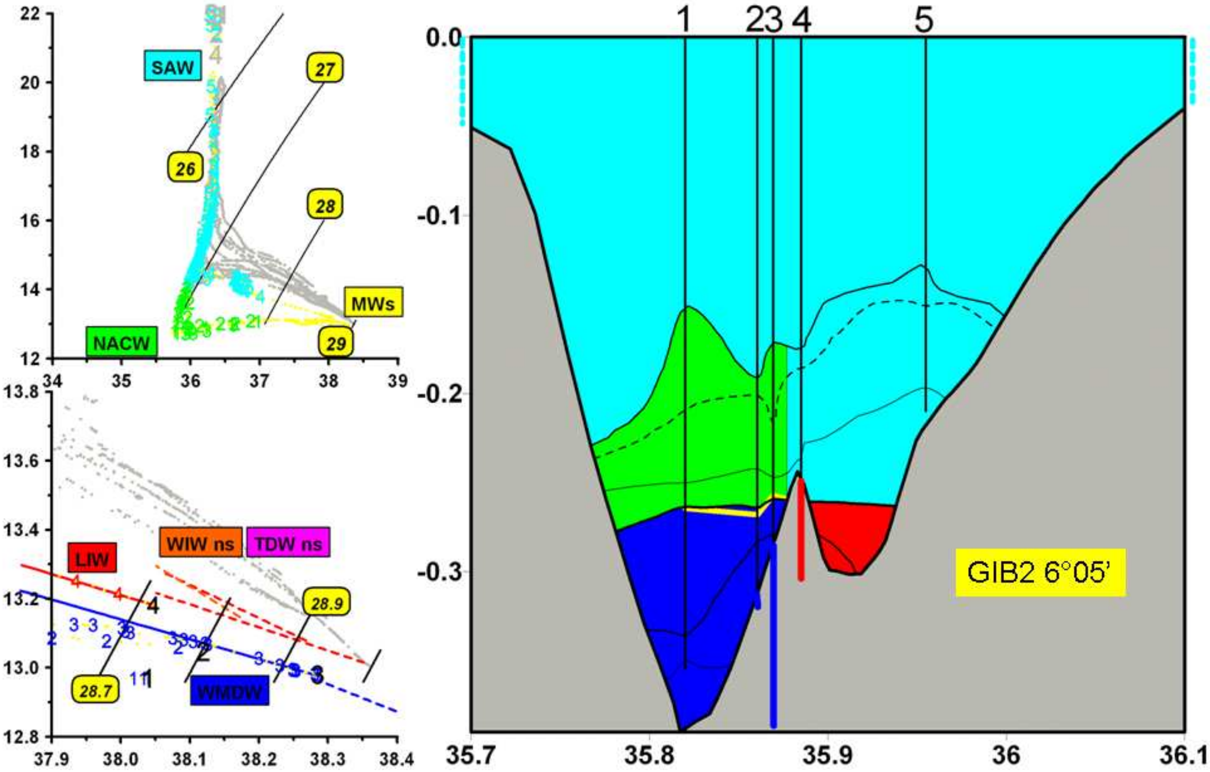

Figure 21

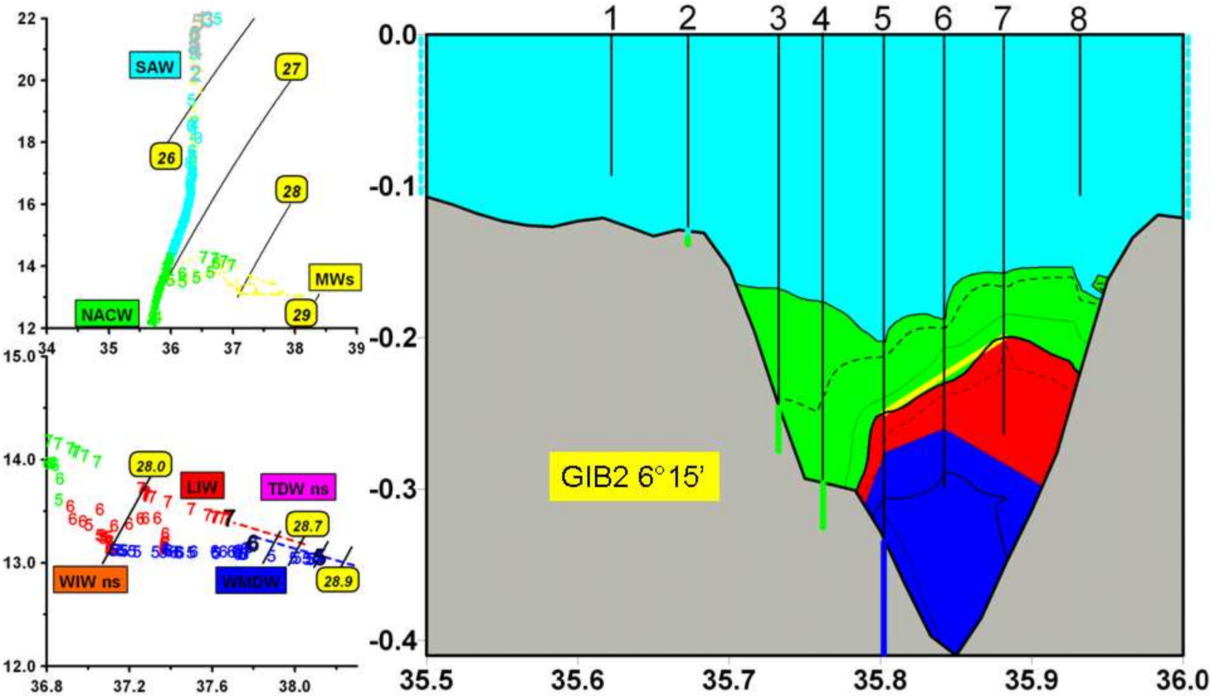

SAW
NACW
MWs
26
27
28
29
LIW
TDW ns
WIW ns
WMDW
28.0
28.7
28.9
1
2
3
4
5
6
7
8
GIB2 6°15'
0.0
-0.1
-0.2
-0.3
-0.4
35.5
35.6
35.7
35.8
35.9
36.0

Figure 22

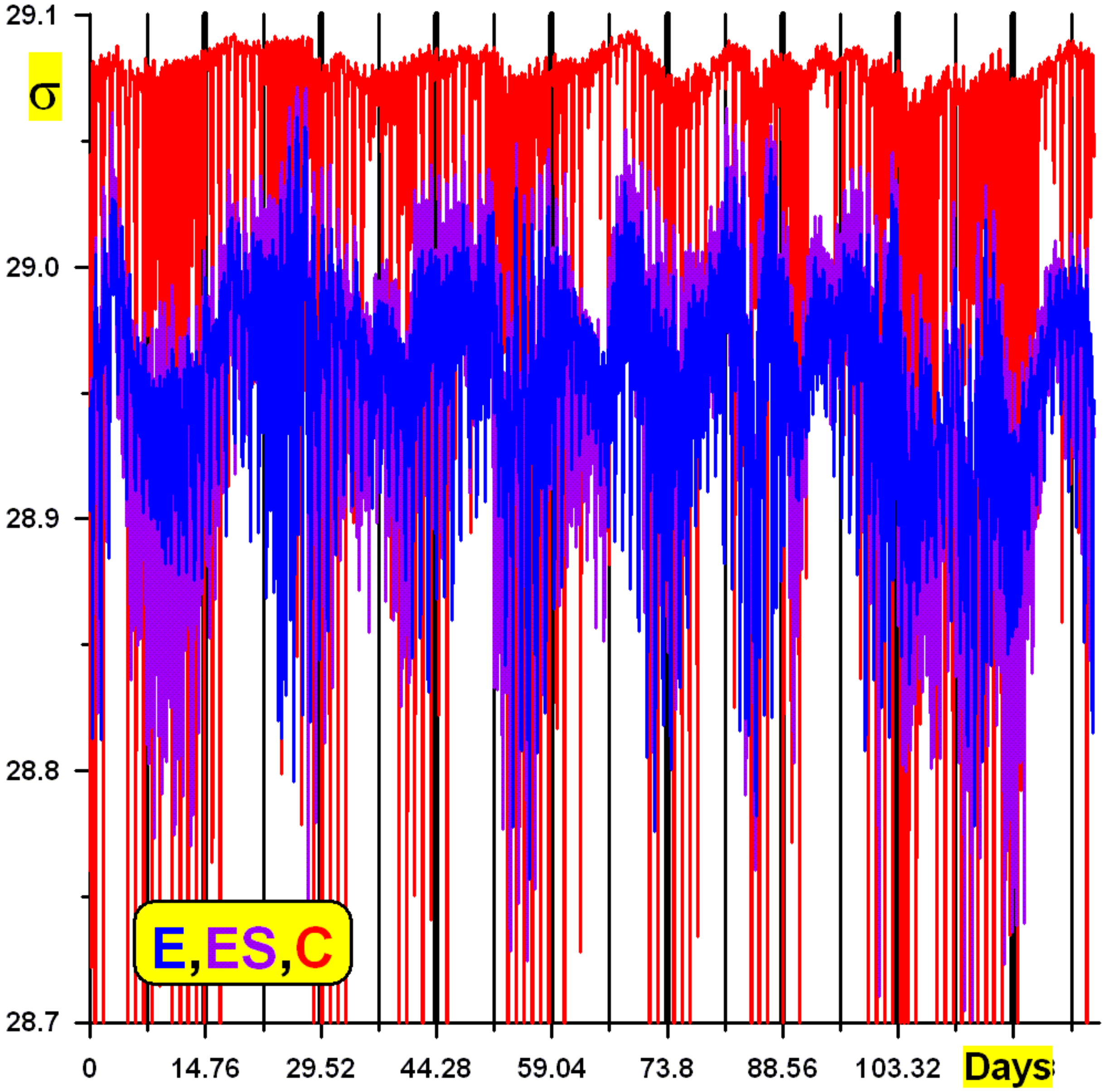
29.1
σ
29.0
28.9
28.8
E,ES,C
28.7
0
14.76
29.52
44.28
59.04
73.8
88.56
103.32
Days

Figure 23

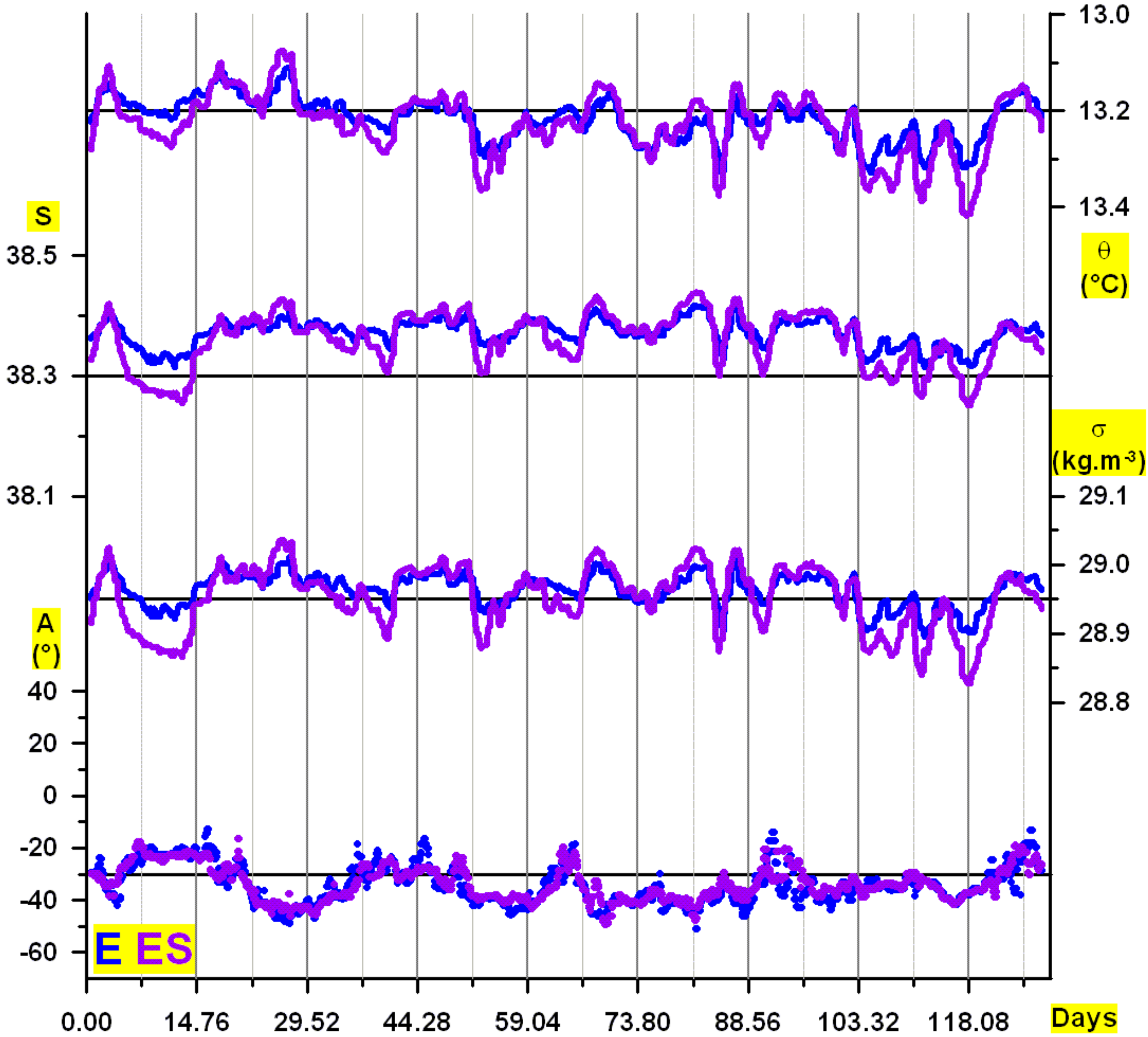

S
38.5
38.3
38.1
A
(°)
40
20
0
-20
-40
-60
E ES
13.0
13.2
13.4
θ
(°C)
σ
(kg.m-3)
29.1
29.0
28.9
28.8
0.00
14.76
29.52
44.28
59.04
73.80
88.56
103.32
118.08
Days

Figure 24

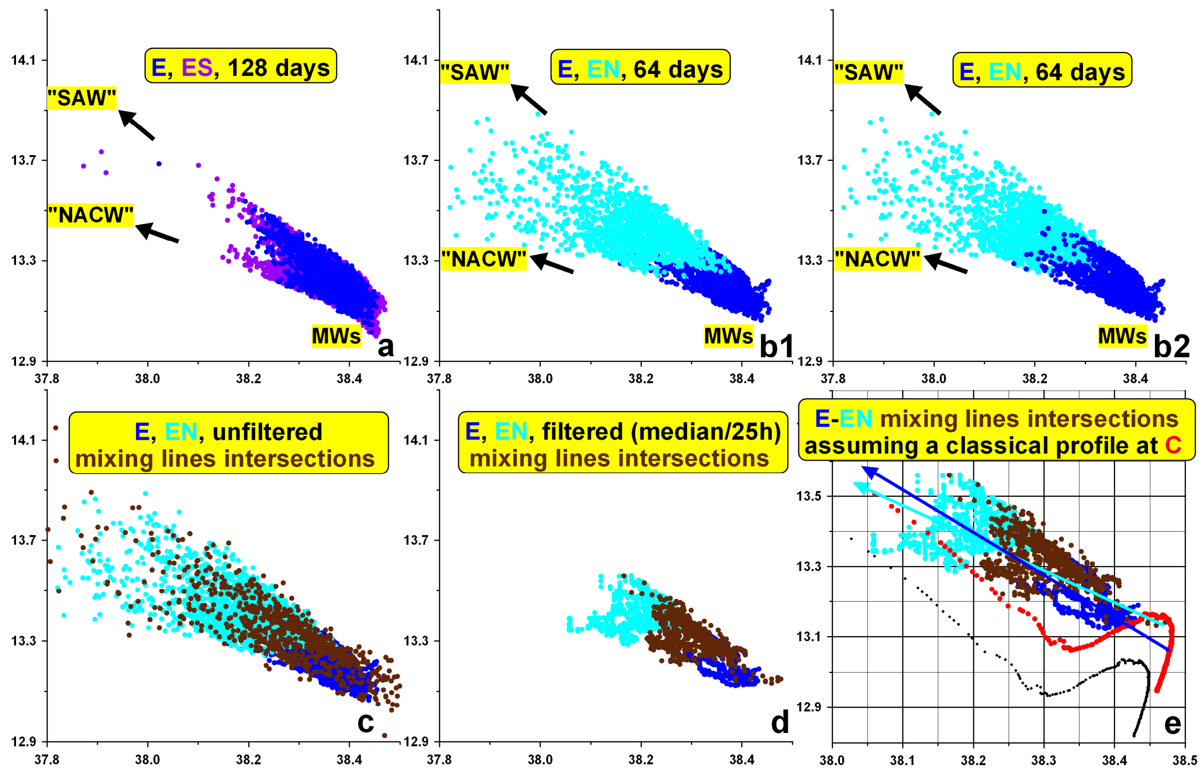
E, ES, 128 days
"SAW"
"NACW"
MWs
a
E, EN, 64 days
b1
b2
E, EN, unfiltered
mixing lines intersections
c
E, EN, filtered (median/25h)
mixing lines intersections
d
E-EN mixing lines intersections
assuming a classical profile at C
e
14.1
13.7
13.5
13.3
13.1
12.9
37.8
38.0
38.1
38.2
38.3
38.4
38.5

Figure 25

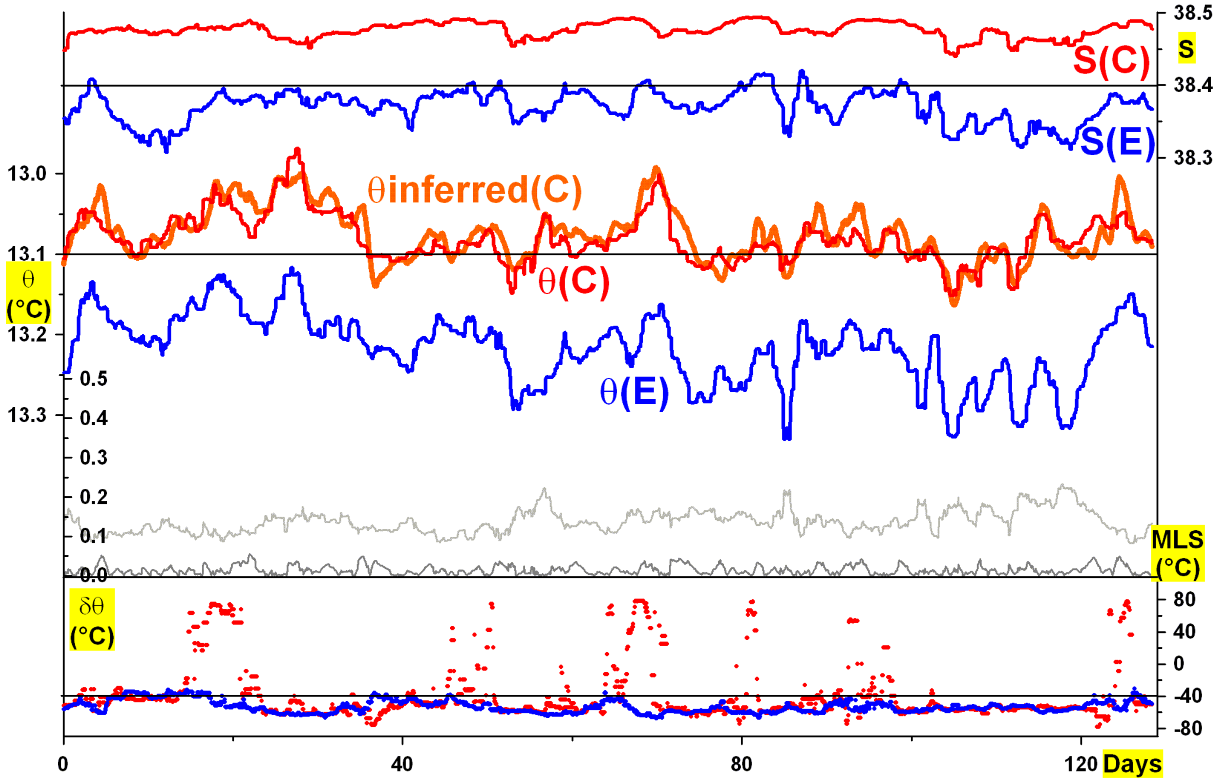

38.5
S
S(C)
38.4
S(E)
38.3
13.0
θinferred(C)
13.1
θ
(°C)
θ(C)
13.2
0.5
θ(E)
13.3
0.4
0.3
0.2
0.1
MLS
(°C)
0.0
δθ
(°C)
80
40
0
-40
-80
0
40
80
120
Days

1
2 Figure 26

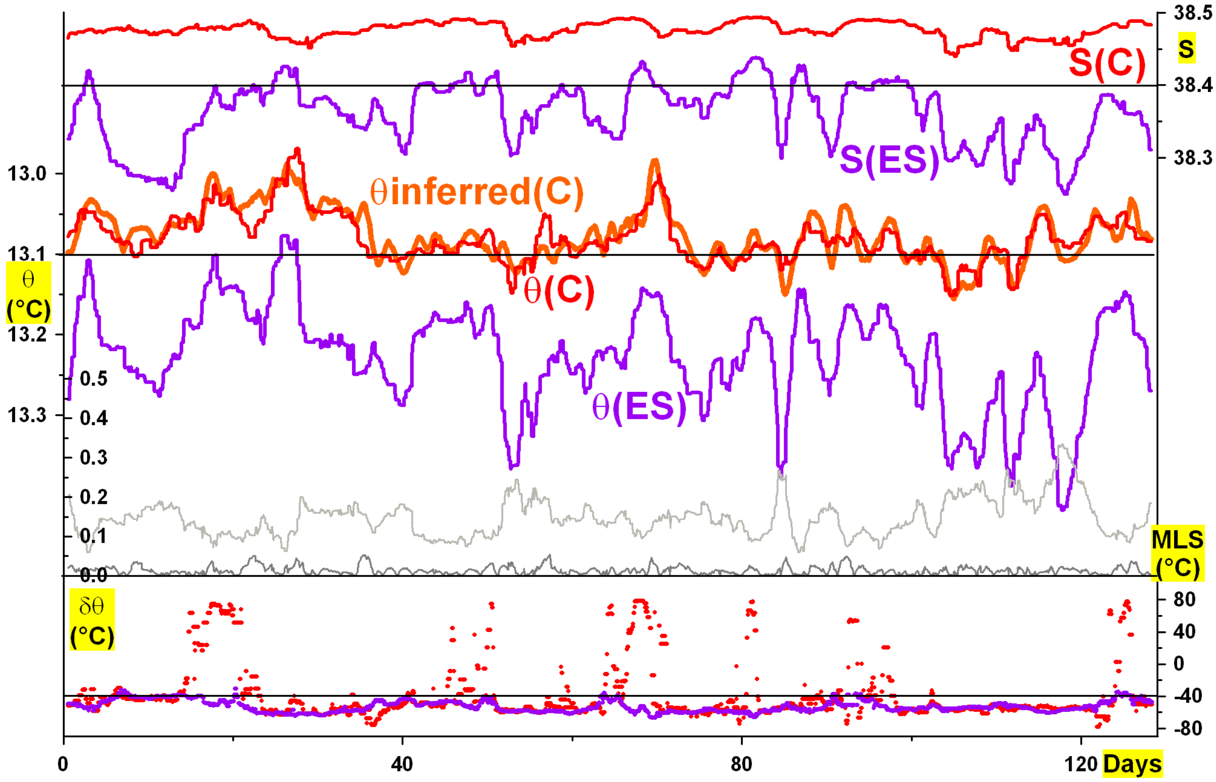
S(C)
S(ES)
θinferred(C)
θ(C)
θ(ES)
θ (°C)
S
MLS (°C)
δθ (°C)
Days
13.0
13.1
13.2
13.3
38.5
38.4
38.3
0.5
0.4
0.3
0.2
0.1
0.0
80
40
0
-40
-80
0
40
80
120

Figure 27

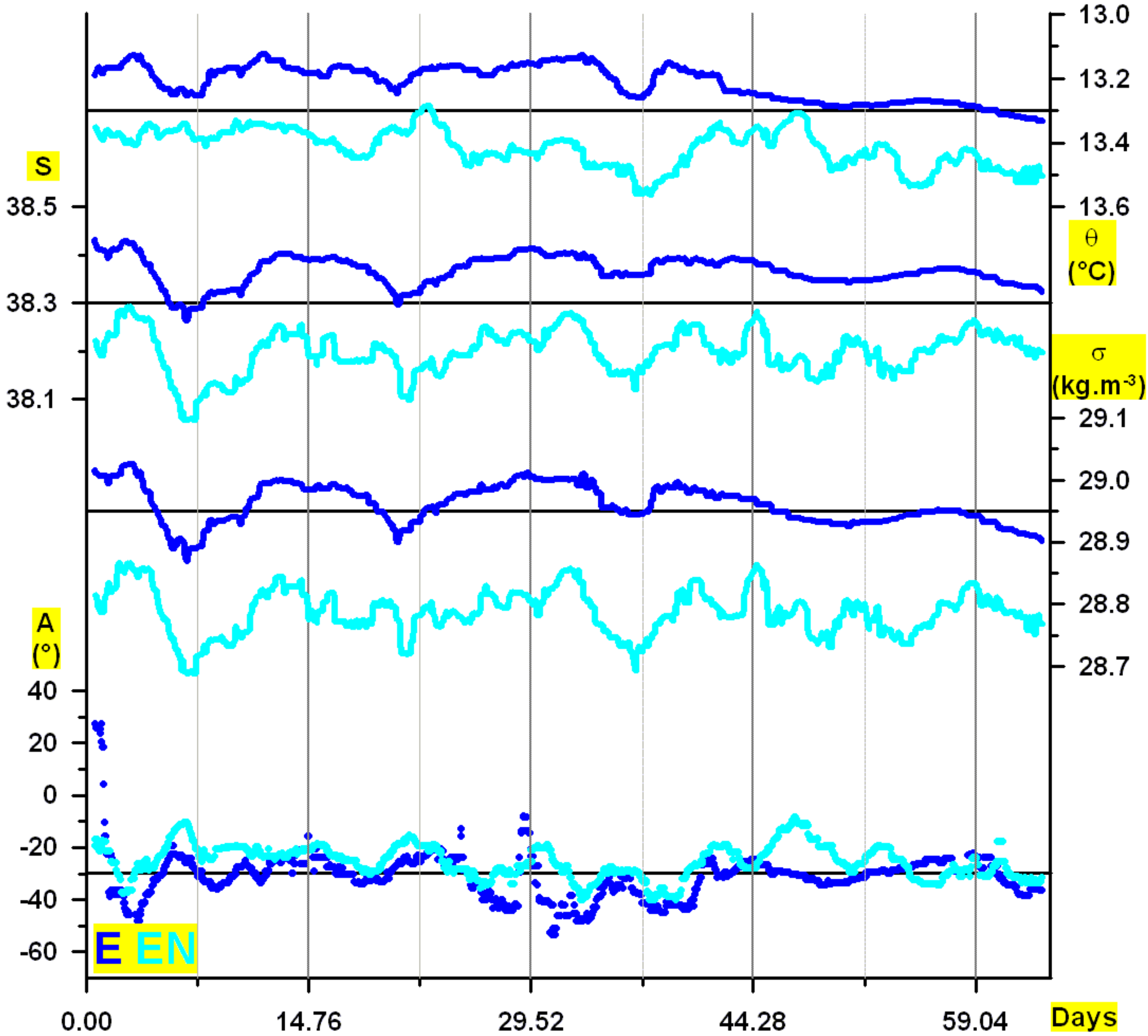
S
38.5
38.3
38.1
θ
(°C)
13.0
13.2
13.4
13.6
σ
(kg.m-3)
29.1
29.0
28.9
28.8
28.7
A
(°)
40
20
0
-20
-40
-60
E EN
0.00
14.76
29.52
44.28
59.04
Days

Figure 28

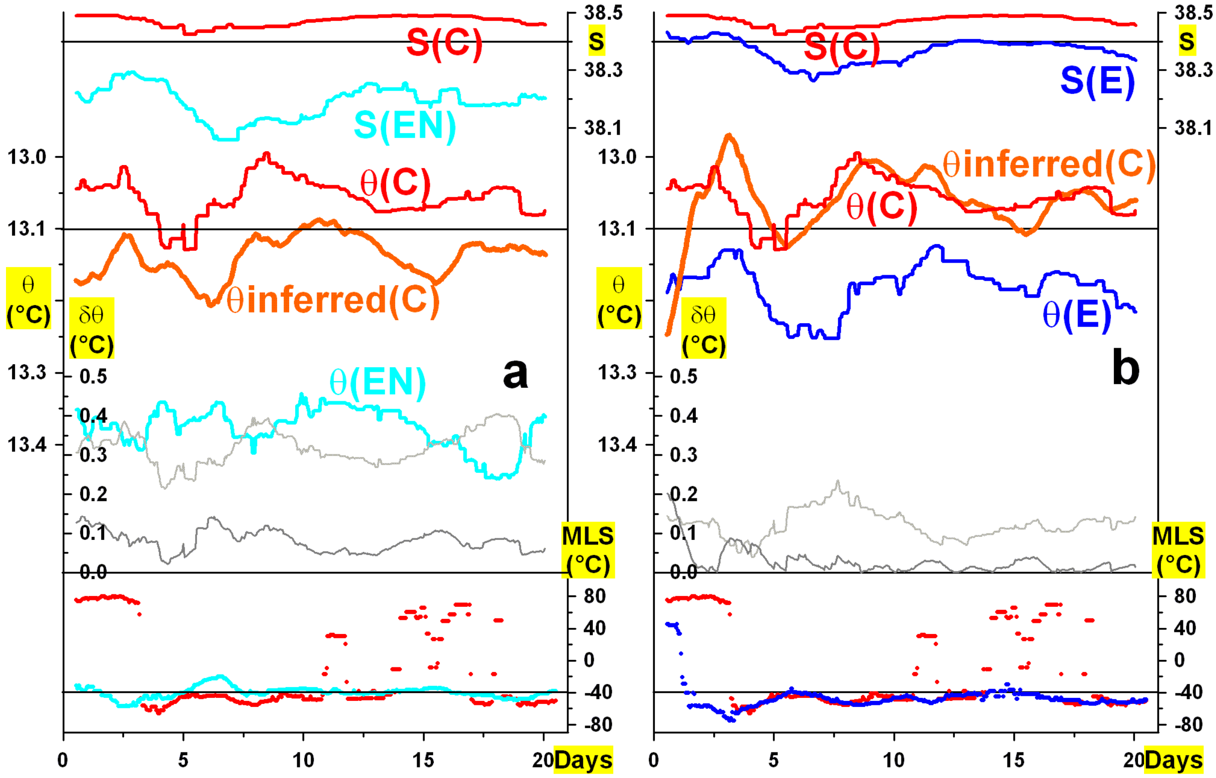
S(C)
S(EN)
θ(C)
θinferred(C)
θ(EN)
a
S(C)
S(E)
θinferred(C)
θ(C)
θ(E)
b
S
38.5
38.3
38.1
θ (°C)
δθ (°C)
13.0
13.1
13.3
13.4
0.5
0.4
0.3
0.2
0.1
0.0
MLS (°C)
80
40
0
-40
-80
0
5
10
15
20
Days

Figure 29

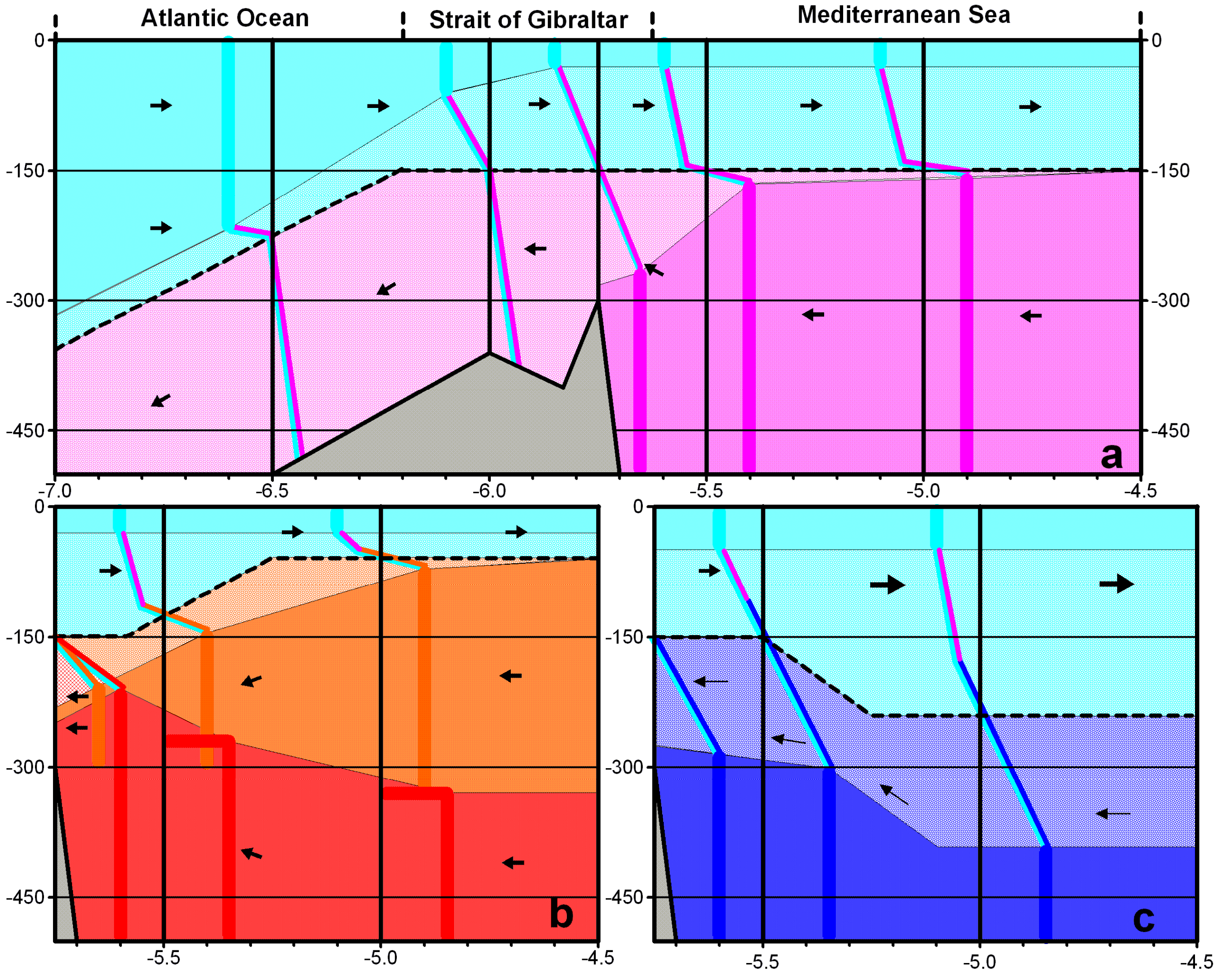
Atlantic Ocean
Strait of Gibraltar
Mediterranean Sea
0
-150
-300
-450
-7.0
-6.5
-6.0
-5.5
-5.0
-4.5
a
b
c

Figure 30

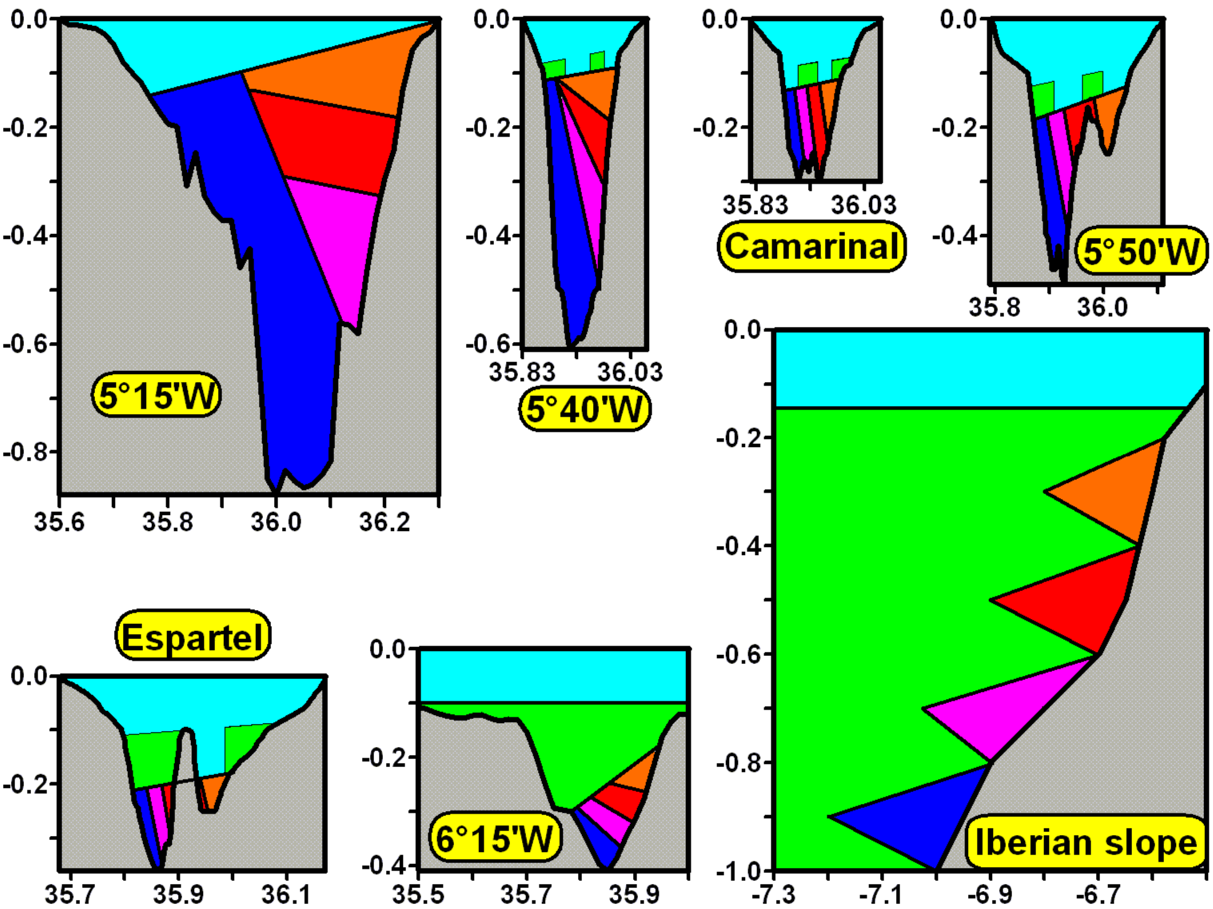
5°15'W
0.0
-0.2
-0.4
-0.6
-0.8
35.6
35.8
36.0
36.2
5°40'W
35.83
36.03
Camarinal
5°50'W
35.8
36.0
Espartel
35.7
35.9
36.1
6°15'W
35.5
35.7
35.9
Iberian slope
-1.0
-7.3
-7.1
-6.9
-6.7

Figure 31